Control of screw pile installation to optimise performance for offshore energy applications

Cerfontaine, Benjamin; Brown, Michael; Knappett, Jonathan; Davidson, Craig; Sharif, Yaseen; Huisman, Marco

Published in:
Géotechnique

DOI:
10.1680/jgeot.21.00118

Publication date:
2021

Licence:
CC BY

Document Version
Peer reviewed version

Submission date:

Title: Control of screw pile installation to optimise performance for offshore energy applications

Author list: Cerfontaine, B.*, Brown, M.J., Knappett, J.A., Davidson, C., Sharif, Y.U., Huisman, M., Ottolini, M., Ball, J.

**Corresponding author*
Author details
*Benjamin Cerfontaine, BSc, MSc, PhD
Lecturer, Engineering and Physical Sciences, University of Southampton, Boldrewood campus, Southampton, UK
ORCID: 0000-0002-4833-9412
Email: b.cerfontaine@soton.ac.uk

Michael John Brown, BEng PhD GMICE
Professor, School of Science and Engineering, University of Dundee, Fulton Building, Dundee,
DD1 4HN, UK
ORCID: 0000-0001-6770-4836
Email: m.j.z.brown@dundee.ac.uk

Jonathan Adam Knappett, MEng (Hons), PhD
Professor, School of Science and Engineering, University of Dundee, Fulton Building, Dundee,
DD1 4HN, UK
ORCID: 0000-0003-1936-881X
Email: j.a.knappett@dundee.ac.uk

Craig Davidson, BSc MSc
Research Associate, School of Science and Engineering, University of Dundee, Fulton Building,
Dundee, DD1 4HN, UK
ORCID: 0000-0002-4843-5498
Email: c.s.davidson@dundee.ac.uk

Yaseen Umar Sharif, MEng
PhD student, School of Science and Engineering, University of Dundee, Fulton Building, Dundee, DD1 4HN, UK
ORCID: 0000-0002-3620-7500
Email: y.u.sharif@dundee.ac.uk

Marco Huisman, MSc PhD
Technology advisor, Heerema Marine Contractors, Leiden, the Netherlands
ORCID: 0000-0001-9704-5843
Email: mhuisman@hmc-heerema.com

Marius Ottolini, MSc
Heerema Marine Contractors, Leiden, the Netherlands
ORCID: 0000-0003-4596-0016
Email: mottolini@hmc-heerema.com

Jonathan David Ball, BSc, CGeol, FGS
Chief Geotechnical Engineer, Roger Bullivant Ltd, Burton Upon Trent, UK
Email: Jon.Ball@roger-bullivant.co.uk

Word count: 6908
Number of Tables: 4
Number of figures: 16

Control of screw pile installation to optimise performance for offshore energy applications

Cerfontaine, B., Brown, M.J., Knappett, J.A., Davidson, C., Sharif, Y.U., Huisman, M., Ottolini, M., Ball, J.

Abstract: Screw piles can be used as foundations for offshore energy applications, thanks to their silent mode of installation and considerable uplift capacity, although a significant upscaling of onshore dimensions will be necessary. However, the crowd (vertical) force necessary to install upscaled screw piles was previously shown to be far too great for practical installation. Whilst guidance recommends that the pile vertical displacement must be one helix pitch (helix height) per each pile revolution, it is shown in this paper that a lower vertical displacement per revolution can significantly reduce the necessary crowd force during installation or even generate some pull-in. In addition, it was shown that the uplift stiffness and capacity of the pile were enhanced by this installation process, at a shallow (relative) depth in sand. This paper gathers nineteen centrifuge tests, with varying screw pile geometries (shaft diameter, base shape), sand relative density and advancement rates. A predictive framework for the pull-in potential of a given pile geometry was proposed to assess its ability to be installed with a reduced crowd force.

Keywords: Offshore engineering, Anchors & anchorages, Centrifuge modelling, sand

1. Introduction

Screw (or helical) piles are composed of one or several steel helices connected to a central shaft or core (Perko, 2009; Lutenegger, 2011). The piles are screwed into the ground by applying a torque at the top of the pile together with a compressive (crowd) force. Currently, screw piles of relatively small dimensions (helix diameter ranging from 150-600 mm; Perko, 2009) are typically used onshore (Tang and Phoon, 2020), e.g. to anchor light structures such as telecommunication towers (Schiavon *et al.*, 2016a), foundations for buildings (Komatsu, 2007), bridges (Harnish and El Naggar, 2015) or modern offshore energy applications (Byrne and Houlsby, 2015; Spagnoli *et al.*, 2020) for which they have three main advantages. Firstly, their embedded helical plate provides significant uplift resistance (Giampa *et al.*, 2017; Hao *et al.*, 2019; Cerfontaine *et al.*, 2020b). Secondly, helical piles are "silently" installed, with very low underwater noise, whereas pile driving associated noise is considered harmful for marine life (Bailey *et al.*, 2010). Finally, they could be removed by reverse rotation (Ding *et al.*, 2019) to allow complete decommissioning.

The design of offshore screw piles or anchors is based on the maximisation of their capacity (depending on embedment depth or helix and shaft diameters), whilst minimising the installation torque and force requirements. To achieve these objectives, offshore piles/anchors will typically have larger shaft and helix diameters than their onshore counterparts (Cerfontaine *et al.*, 2020a). They will also be installed at a lower relative embedment depth. However, Davidson *et al.* (2020) have shown that the crowd force necessary to install (in a pitch-matched manner, see below) upscaled piles to found jacket structures in sand tends towards the upper limit of the reaction force that could practically be achieved by an installation vessel and could lead to pile instability and/or buckling.

The advancement ratio (AR) is used to describe the installation of screw piles (Bradshaw *et al.*, 2018; Sharif *et al.*, 2020a). It is calculated as the ratio of the vertical pile displacement for one helix revolution (Δz_h) to the helix pitch (p_h), defined as the height of the helix measured at mid-plate (Figure 1).

$$AR = \frac{\Delta z_h}{p_h} \quad (1)$$

It is recommended that the AR of a pile should be greater than 0.8 (Perko, 2009) or within 1±0.15 (BS8004:2015, 2015), i.e. the pile advances one helix pitch for each helix revolution. This installation is termed 'pitch-matched' and is suggested with the supposed aim of reducing the soil disturbance during installation. Such disturbance is always considered to be detrimental. Schiavon, (2016) showed that even a pitch-matched installation loosened the soil above the helix, which can create a weak zone in which an uplift failure mechanism will develop (Schiavon *et al.*, 2016b). Nagai *et al.* (2018) showed that alternating foreward and backward rotation of the helix decreases the uplift capacity.

Results of field tests (Richards *et al.*, 2018) and small-scale constant crowd force installation (Bradshaw *et al.*, 2018) where the AR was carefully measured, showed that the AR decreased with depth and reached an asymptotic value significantly lower than 1. This suggests that screw pile installation at an AR lower than 1, referred to hereafter as overflighted, has the potential to reduce the necessary crowd force and may be commonplace in field practice. This has been demonstrated by numerical modelling for single helix screw piles (Sharif *et al.*, 2020a) and small-scale 1g tests (Wang *et al.*, 2020). It was also shown by Sharif *et al.* (2020a) using DEM modelling that pile overflighting could have a beneficial effect on the pile uplift capacity, although at the expense of a reduced compressive capacity. On the contrary, Wang *et al.* (2020) undertook small-scale 1g tests in sand at very shallow embedment ratios (H/D_h = 2.6, 3.3 and 4.4) and showed a reduction in the uplift capacity for overflighted piles.

To predict the screw pile force and torque installation requirements, analytical or semi-analytical models are required to ensure installation feasibility and mobilisation of adequate installation plant. Several models have been developed (Tsuha and Aoki, 2010; Sakr, 2015; Davidson *et al.*, 2020; Spagnoli *et al.*, 2020), but these are all based on the explicit hypothesis of a pitch-matched (AR = 1) installation. Therefore, there is a need for a new framework, including the AR effect which enables a more accurate prediction and optimisation of the installation process.

This paper investigates how screw pile installation requirements (force and torque) and uplift capacity/stiffness in sand change as a function of a fixed AR imposed during installation. It will be demonstrated by centrifuge testing that overflighting screw piles in sand reduces the crowd force necessary for installation, without degrading the uplift capacity. Nineteen centrifuge tests were undertaken, varying the sand density (medium-dense or dense), the advancement ratio, and the pile geometry (core diameter at fixed helix dimensions, pile base shape and helix pitch). A theoretical model is developed to explain the AR effect on the pile capacity and an empirical framework is introduced to summarise the experimental results and enable a fast estimation of the reaction force requirements for pile installation.

2. Methodology

2.1. Centrifuge set-up

The centrifuge tests were performed using the Actidyn C67-2 3 meter radius geotechnical beam centrifuge located at the University of Dundee (UK). Previous investigations of the effects of installing model piles at 1g before subsequent testing at high-g levels revealed significant differences in the response of the model pile compared to in-flight installation and testing (Klinkvort *et al.*, 2013). Therefore, equipment was developed at the University of Dundee which is capable of installing and testing screw piles in one continuous centrifuge flight (Al-Baghdadi *et al.*, 2016; Al-Baghdadi, 2018; Davidson *et al.*, 2020). The testing equipment enabled precise

control of the rotational and vertical displacement of the model piles, powered by two servo-motors. A load cell measured the torque from – 30 Nm to +30 Nm and the axial force from -20 kN to +20 kN at the top of the pile model. The axial displacement was measured by a draw wire transducer. Further details can be found in Davidson *et al.* (2020).

2.2. Sand bed preparation

Medium-dense and dense sand beds (425 mm deep) were created by dry pluviation of HST95 sand in a strong box (500 mm x 800 mm x 550 mm). The HST95 sand is a fine-grained quartz sand whose properties are given in Table 1. It has been extensively used and characterised at the University of Dundee for laboratory testing (Lauder, 2010; Al-Defae *et al.*, 2013; Robinson *et al.*, 2019) and used in previous screw pile investigations. A linear pluviator was mounted on rails running above the container at a constant velocity. The sand was pluviated to just above the target height, and the sand surface was levelled. Medium-dense (sand bed average relative density D_r 52-53%) and dense (D_r 72-78%) sand beds were prepared. All tests were undertaken in dry conditions. Additional information on sample preparation and in-flight CPT profiles can be found in (Davidson *et al.*, 2020).

2.3. Pile models

A total of 19 different centrifuge tests (Table 2) were undertaken for five pile geometries (Figure 1a). A scaling factor of 50 was used to calculate prototype dimensions. All models were made from steel and had solid cores to avoid premature plugging of small-scale open-ended piles. The helix diameter (D_h, 1.06 m at prototype scale) and its final embedment depth (H_{base} = 7.5D_h) were identical in all test. The embedment depth corresponded to a shallow mechanism in uplift, but was close to the limit for shallow to deep mechanism formation (in the range $5D_h$-$8D_h$ (Cerfontaine *et al.*, 2019)). The geometry and embedment depths are considered representative of anchors for floating wave or tidal offshore energy devices, whilst groups of them should be used for floating wind turbines (Cerfontaine *et al.*, 2020a).

The flat based reference pile (P1 in Figure 1a), was used in a previous study by Davidson *et al.*, (2020). The helix plate thickness was equal to 0.07 m (1.4 mm at model scale) to ensure helix structural integrity. Additional piles were manufactured to investigate the effect of key parameters such as shaft diameter or base shape (asymmetric, i.e. cut at an angle of 45 ° to the horizontal direction) on the installation requirements and anchor capacity.

Two tests were undertaken in each container/sand bed (Figure 1b), with manual repositioning of the actuator after the first test where centrifuge spin up and spin down were required between tests. The spacing between the closest boundary and each pile was approximately 12 times the helix diameter (or 23 shaft diameters). This is larger than the minimum distance of 10 recommended by Bolton *et al.* (1999). The distance between the pile and the boundary is also 5 times the largest dimension of a wedge failure mechanism at the sand surface that could be expected for shallow uplift mechanisms (Giampa *et al.*, 2017). The ratio of the minimum shaft diameter to the average particle diameter (D_s/D_{50}) was equal to 57, which is larger than the recommendation of 44 (Garnier *et al.*, 2007). Similarly, the helix diameter to average particle size ratio (D_h/d_{50}) is equal 152, which is larger than the recommendation of 48 (Garnier *et al.*, 2007). Schiavon *et al.*, (2016b) introduced an additional criterion to verify of particle scale effects during screw pile installation. They calculated the ratio of the effective helical radius dimension ($w = (D_h - D_s)/2$) to the average grain size (d_{50}), to verify enough particles are in contact with the helix. However, the authors did not propose a lower bound where particle scale effects occur i.e. their lower bound value ($w/d_{50} = 58$) only reflected the range of their investigation. Further tests by Rafsanjani *et al.* (2021) did not identify scale effects on the uplift capacity for $w/d_{50} > 16$. This ratio (w/d_{50}) varies between 26 and 47 in this study.

2.4. Testing procedure

The tests were undertaken at 1:50 scale. After spinning to 50g, installation of the pile was undertaken at constant rotation rate (3RPM) and the vertical velocity was chosen to impose a given AR. The vertical velocity was adjusted for each test to achieve the desired advancement ratio (AR) and was kept constant over the entire installation process. Once the pile helix reached the target depth, the vertical and rotational movements were stopped. The applied torque was released, which in turn modified the vertical force measured at the end of the installation, with a slight shift to compression. Finally, the pile was subjected to a tensile load test (uplift velocity: 1 mm/min). The vertical force and torque were zeroed prior to installation when the pile was freely hanging below the actuator at 50g (prior to surface penetration). Therefore, the measured uplift capacity is only due to the soil resistance. All data in this paper are available in open-access at Cerfontaine (2021).

3. Results & discussion

3.1. Effect of Advancement Ratio (AR)

3.1.1. *Effect on the measured vertical force (F_z)*

The vertical force (F_z) acting on the reference pile (P1, flat base shape) during installation is shown in Figure 2 in dense and in medium-dense sand, for different advancement ratios. Both figures show that a significant compressive force (negative sign in Figure 2) is necessary to achieve the ARs recommended by the standards (AR =1±0.15, according to BS 8004 (2015)), i.e. to achieve a pitch-matched installation. Such large compressive forces were also observed by Davidson *et al.* (2020) for pitch-matched installation. When subjected to lower advancement ratio (AR $\leq$0.5), tension was measured by the load cell, indicating the pile can pull itself in. This reduction in force is consistent with small-scale 1g tests at constant ARs $\leq$1 (Wang *et al.*, 2020).The change of behaviour from compressive (AR > 0.5) to tensile (AR ≤0.5) vertical installation force is quite abrupt rather than a smooth transition. There is a jump in the results from significant compressive force (AR = 0.8) to almost zero installation force (AR = 0.5). The

compressive vertical force keeps increasing as the AR increases from AR =0.8 to 1.0, but there is only a marginal increase in tension for AR = 0.25 to 0.1. These observations suggest that two different mechanisms are developing as a function of the applied AR.

3.1.2. *Idealisation of the installation mechanism*

To understand the AR effect on installation, it must be kept in mind that the helix (F_h), the shaft (F_s) and the base (F_b) forces (Figure 3) all contribute to the total penetration resistance in different proportions (Tsuha and Aoki, 2010; Sakr, 2015; Davidson *et al.*, 2020). The most significant change in penetration resistance with AR is due to the helix rotating and vertical movements. DEM simulations (Sharif *et al.*, 2020a) have shown that pile overflighting induced an upwards displacement of soil particles during their installation together with a reduction in vertical force. To the authors' knowledge, there is no theoretical model in the literature that describes the overflighting of screw piles. However, the overflighting of continuous flight auger (CFA) piles has previously been considered (Mandolini *et al.*, 2005), where overflighting leads to a vertical displacement of particles by the helical thread (augering) and a decompression of the soil under the pile.

Based on this insight, Figure 4 shows an idealisation of the helix and particle movement. The helix edge is shown unfolded in 2D (depicted by a solid black line in Figure 4a-b) and its initial position (Figure 4a) is assumed to be in contact with some particles along its upper and lower faces. The displacement of a pitch-matched helix (AR = 1.0), would be parallel to the helix. The displacement of an overflighed helix (AR = 0.5 in this case) has a different displacement vector, as represented in Figure 4b. Consequently, unloading of contact forces on the lower face of the helix is promoted. The particles initially in contact with the helix upper face are forced to move upwards by the helix rotation. The displacement of the helix during one revolution (Δz_h) is related to the advancement ratio (AR) and the helix pitch (p_h) after Equation

(1). The particle maximum vertical displacement along the helix during one revolution (Δz_p) is calculated as

$$\Delta z_p = (1 - AR) \cdot p_h \quad (2)$$

A pitch-matched installation (AR = 1) would induce limited particle displacement, hence minimising the disturbance, and explains the origin of recommendations (BS8004:2015, 2015). A purely rotating pile (no vertical pile displacement, AR = 0) would maximise the particle displacement (upwards or laterally depending on the helix parameters and soil conditions). However, this reasoning does not consider that disturbance can have a beneficial effect, by enhancing the stress state.

In Figure 4b, particles are free to be moved vertically (AR<1), but when the helix is embedded, particles are prevented from moving upwards by the surrounding soil. It is assumed that this soil acts as a non-linear spring (Figure 4c) upon which an imposed displacement is applied, which creates a reaction force. The reaction force acts downwards on the helix and creates the tension force that was measured in the pile during the experiment (F_z>0 in Figure 2), i.e. the helix contribution (F_h) changes from a penetration resistance to an active pull-in force. This pull-in is the average of the non-homogeneous stress distribution (i.e. particle displacement dependent) acting on the helix. In addition, the potential for reduction in contact force beneath the helix induces a reduction of the vertical stress in the soil beneath the helix (Figure 4b-c). This in turn reduces the base penetration resistance (F_b) by removing the overburden effect on the pile base penetration mechanism. The reduction in vertical force and reduction in stress below the helix during the installation have both been observed in DEM simulations for a single helix screw pile (Sharif *et al.*, 2020a).

The shaft penetration resistance (F_s) is only due to the vertical shear stress (τ_z) along the pile-soil interface (Figure 3). Rotary movement of piles has been shown to decrease τ_z due to a

change of shear stress orientation (Figure 3) (Deeks, 2008; Sharif *et al.*, 2020b). If σ_r is the radial stress acting on the shaft at a given depth, the maximum shear stress that can be mobilised is equal to

$$\tau_{max} = \sigma_r \tan \delta_{crit} \tag{3}$$

where (δ_{crit} is the interface critical state friction angle). This maximum shear stress would be oriented vertically along the shaft of a jacked pile. For a rotary installation, Deeks *et al.* (2010) proposed that the orientation of the shear stress (τ_{max}) is parallel to the instantaneous velocity of the pile (v_i), as shown in Figure 3. If the radial stress is assumed independent of AR, the shear stress horizontal and vertical components (τ_h, τ_z) are then calculated as

$$\frac{\tau_h}{\tau_{max}} = \frac{p_i}{\sqrt{1 + p_i^2}} \tag{4}$$

$$\frac{\tau_z}{\tau_{max}} = \frac{1}{\sqrt{1 + p_i^2}} \tag{5}$$

where the installation pitch p_i is defined by Deeks *et al.* (2010) as

$$p_i = \frac{v_h}{v_z} = \frac{\omega D_s}{2v_z} = \frac{\tau_h}{\tau_z} \tag{6}$$

where ω is the angular velocity of the pile. It must be pointed out that the installation pitch (p_i) is an installation parameter that describes the shaft movement and is independent of the helix geometric pitch (p_h). The relationship between the AR (related to the helix) and the installation pitch (related to the shaft) only depends on geometric parameters.

$$p_i = \frac{\pi D_s}{p_h AR} \tag{7}$$

Figure 5a shows the effect of variation of AR on installation pitch (Equation (7)). It shows that the relationship between the installation pitch and the AR is only dependent on the shaft diameter to helix pitch ratio (D_s/p_h) and strongly increases as AR decreases. For the reference pile geometry (P1, $D_s/p_h = 1.5$), Figure 5b shows that the vertical shear stress for pitch-matched conditions (AR = 1) is reduced to 21% of the maximum shear stress, but drops to only 1% at AR = 0.1. This reduction in vertical shear stress is directly linked to a reduction in shaft penetration resistance (F_s).

3.1.3. *Effect on the measured torque*

The torque (T) measured during the pile installation (Figure 6) exhibits less variation as a function of AR than the force. In dense sand (Figure 6a), the largest torque is measured for an AR of 0.5, while the lowest AR (0.1) leads to the largest torque in medium-dense sand (Figure 6b). The torque can be decomposed into shaft (T_s), base (T_b) and helix (T_h) that are all directly related to the force components (Figure 3).

The torque acting on the shaft (T_s) is proportional to the horizontal shear stress (τ_h in Equation 4) and the lever arm ($D_s/2$). The shaft component increases non-linearly with depth as both the surface of the embedded shaft and the radial stress magnitude increase. The base (T_b) and helix (T_h) torque components can be calculated as the vertical force (F_b and/or F_h) multiplied by an equivalent lever arm (Tsuha and Aoki, 2010) if the pile behaviour is dominated by one face of the helix: lower face in compression and upper face in tension. Figure 2 showed that the large compressive force (tests where AR>0.5) increases almost linearly with depth. The torque for the same tests evolves also approximately linearly (Figure 6), which suggests that the base and helix contributions are dominant for the torque behaviour at larger ARs.

The torque in dense sand (Figure 6a) is maximum for AR = 0.5, while the vertical force is almost equal to zero (Figure 2a). In this case there is no linear relationship between force and torque. This apparent paradox can be explained as follows. The force acting on the helix (F_h) is the sum of forces acting on its lower and upper faces. There exists a configuration in which

those forces are equal in magnitude and opposed in sign, leading to zero resultant force. On the contrary, the torque associated with each vertical force adds up.

The measured torque for the other tests (AR < 0.5) becomes more non-linear with depth. This is consistent with the overflighting effect as explained in the previous section (3.1.2). When the soil is compressed vertically due to the overflighting movement, it also increases the radial stress acting on the shaft in the vicinity of the helix. Therefore, the more pull-in the helix will create, the greater the radial stress/torque increase will be along the shaft. However, more tests using instrumented pile would be necessary to quantify the relative contributions of each part of the pile.

3.1.4. *Effect on the uplift capacity*

For all tests, the uplift load-displacement relationship reached a peak or a plateau before softening took place, as shown in Figure 7. This is consistent with previous field tests (Gavin *et al.*, 2014) and wished-in-place centrifuge tests (Hao *et al.*, 2019). Figure 7 shows that reducing the AR was beneficial for the pile uplift behaviour with respect to the pitch-matched installation (AR =1). The stiffness increased and the failure was more ductile than the pitch-matched installation. In all cases, the uplift capacity (peak force) of overflighted piles was greater than those which were pitch-matched installed. This contradicts the recommendations which suggest that overflighting is always detrimental to uplift capacity (Perko, 2009; BS8004:2015, 2015). Results in Figure 7 are also different from Wang *et al.* (2020), who showed a reduction in uplift capacity with a reducing AR. However, those authors tested their piles at much shallower depth and very low stress level. The low stress level might have limited the pull-in effect during the installation, which could explain the difference in observations. Figure 7 also seems to show an initial density effect, as the capacity is optimal for AR = 0.5 in dense sand (Figure 7a), whilst it is maximum for AR = 0.1 in medium-dense sand (Figure 7b).

The peak uplift capacity has been identified for all advancement ratios in both densities and represented by a non-dimensional breakout factor (N_γ) to enable comparison with literature results

$$N_\gamma = \frac{4F_{z,u}}{\gamma' H \pi D_h^2} \tag{8}$$

where *H* is the helix embedment depth, $F_{z,u}$ the total uplift capacity and γ' is the buoyant unit weight (dry weight here). Figure 8a shows that the experimental results (especially for AR = 1) are consistent with the theoretical solution (assuming shallow mechanism) proposed by Giampa *et al.* (2017) developed for pitch-matched installation,

$$N_\gamma = 1 + 2\kappa \frac{H}{D_h} + \frac{4}{3}\kappa \tan\psi_p \left(\frac{H}{D_h}\right)^2 \tag{9}$$

$$\kappa = \tan\psi_p + \cos(\phi_p - \psi_p)(\tan\phi_p - \tan\psi_p) \tag{10}$$

where ϕ_p is the peak friction angle of the soil, ψ_p is the peak dilatancy angle, function of the sand density and stress level (Bolton, 1986). Figure 8a shows that the effect of the AR on the uplift capacity is more pronounced in medium-dense than in dense sand. One explanation could be that medium-dense sand has a greater potential for densification than an already dense sand. However, more tests would be necessary to determine the origin of this difference and its evolution with depth.

3.1.5. *Torque correlation factor*

Torque correlation factors have widely been used to assess the capacity of screw anchors after their installation (Perko, 2009; Tsuha and Aoki, 2010; Harnish and El Naggar, 2015). Byrne and Houlsby (2015) proposed a non-dimensional version of this correlation factor (k_T^*):

$$k_T^* = \frac{F_{z,u} D_h}{T} \quad (11)$$

where T is the torque measured at the end of the installation. The correlation factor has been calculated in all cases (capacity $F_{z,u}$ calculated at peak tensile force or at 10%D_h displacement) and compared with the value recommended by Perko (2009), which is a function of the shaft diameter. Figure 8b shows that some variability can exist as a function of the advancement ratio, but also that there is a significant difference in torque correlation factor as a function of relative density. This factor was also shown by Sharif *et al.* (2020b) in DEM studies to decrease as a function of the helix embedment depth and to increase as AR decreases ($0.5 \leq AR \leq 1.2$), although no peak of k_T^* was reported by those authors. The total torque (T) and uplift capacity ($F_{z,u}$) will be affected in different ways by the AR and depth and are likely to produce different values of k_T^*. Consequently, it is recommended to use such correlation factors with caution, especially at shallow depths and for larger pile dimensions, which are conditions different from the common practice.

The AR effect on uplift behaviour could be explained as follows. Installation requiring a significant compressive force (large AR, Figure 9a) will generate some loosening of the soil in a cylindrical zone above the helix up to the surface, which has been confirmed by micro-tomographic investigations (Schiavon, 2016; Pérez *et al.*, 2018) and DEM simulations (Sharif *et al.*, 2020a). The large compressive force will generate a high magnitude stress field under the helix, while the stress above the helix will decrease in magnitude, as confirmed by DEM simulations (Sharif *et al.*, 2020a). Installations creating a tensile force (low AR, Figure 9b) have the opposite effect. The imposed displacement of particles upwards creates beneficial soil disturbance and increases the stress magnitude above the helix (Sharif *et al.*, 2020a).

FE analyses have shown that increasing sand density and/or the initial stress magnitude above the helix enhances uplift stiffness and capacity (Pérez *et al.*, 2018; Cerfontaine *et al.*, 2020b).

It is believed that the uplift capacity enhancement observed in the centrifuge tests (e.g. Figure 7) at low AR is due to the uplift failure mechanism developing in a soil which has a greater stress magnitude (Figure 9c) and potentially greater density than the initial state, because of the installation process. In fact, the disturbance created during the installation is a perturbation of the initial soil state (density, stress), but has a beneficial effect on the uplift capacity when the pile is overflighted. However, the full characterisation of the AR effect as a function of depth, sand initial density and persistence in time requires further investigation. This could be undertaken by micro-tomographic scans to investigate the density and pressure sensors to measure radial stress.

3.2. Effect of different shaft diameters

Increasing the shaft diameter (D_s) enhances the shaft lateral and torsional capacities, but also the installation requirements. Piles P4, P2 and P5 consider this with different shaft diameters $D_s = D_h/3$, $D_h/2$ and $2D_h/3$, respectively. These piles also have an asymmetric base shape (45° cut surface), more representative of field piles (Harnish and El Naggar, 2015). As the uplift capacity is mainly driven by the helix diameter (D_h = 1.06 m) and embedment depth, both were maintained constant in these comparisons.

A significant compressive force was necessary to ensure a pitch-matched installation (AR = 1), as shown in Figure 10a. This figure shows that the compressive force was reduced as the helix area increases (shaft decrease), indicating that the shaft diameter and not the helix area controls the increase of the crowd force. However, the same compressive force was measured for the two largest shaft diameters ($D_s = D_h/2$ and $2D_h/3$) installed at AR = 1, suggesting an upper bound in penetration resistance at a given AR. Torque (AR = 1), however, increases continuously with the shaft diameter (Figure 10b). The overflighted piles (AR = 0.5) exhibited different behaviour ranging from compressive vertical force ($D_s = 2D_h/3$) to tensile forces ($D_s = D_h/2$ or $D_h/3$)(Figure 10a). The torque related increased with shaft diameter, but there was only a slight difference between the two largest diameters (Figure 10b).

The increasing dimension of the shaft surface alone is insufficient to explain the observed difference in behaviour as a function of AR, but a theoretical model developed for CFA piles by Viggiani (1989) provides additional insight. The penetration and rotation of the pile create two different mechanisms around the helix (Figure 11d). The pile base penetration displaces a volume of soil laterally (volume V_p), typically analysed using cavity expansion for piles (White and Deeks, 2007). The helix moves a volume of soil (V_h) upwards (AR<1), as previously described. If v_z is the vertical velocity (m/s) of the pile, n_{rot} is the number of revolutions per unit time (s^{-1}) and Δt is an arbitrary duration during which the pile is rotated:

$$\mathrm{V_p} = v_z \frac{\pi D_s^2}{4} \Delta t + \frac{\pi}{4}\left(D_h^2 - D_s^2\right) t_h n_{rot} \Delta t \tag{12}$$

$$\mathrm{V_h} = \frac{\pi}{4}\left(D_h^2 - D_s^2\right)\left(n_{rot}\mathrm{p_h} - \mathrm{v_z}\right)\Delta t \tag{13}$$

where V_p accounts for the volume displaced by a thick helix plate. If the volume displaced laterally (V_p) is lower than the volume displaced vertically (V_h), the pull-in conditions described in the previous sections are met. Particles are displaced predominantly upwards by the helix and a tension force is created in the pile (Figure 11a). On the contrary where compressive forces are generated ($V_h < V_p$), particles are forced to move through the helix but to a lesser extent as a flow around mechanism also develops (Figure 11b-c). This removes the tendency for the contact force to unload beneath the helix and a compressive force becomes necessary to install the pile. Such displacement patterns were reported by Sharif *et al.* (2020a) and Shi *et al.* (2019) who undertook DEM simulations of screw piles. Consequently, the pull-in effect is not only a function of AR (>1 or <1), but also of the pile geometry.

Rearranging Equations (12-13) considering $V_h = V_p$ and assuming an incompressible soil, the critical advancement ratio (AR_{crit}) is defined as

$$AR_{crit} = \frac{v_{z,crit}}{n_{rot} p_h} = \left[1 - \left(\frac{D_s}{D_h}\right)^2\right]\left(1 - \frac{t_h}{p_h}\right) \quad (14)$$

Piles installed with $AR > AR_{crit}$ will require a compressive crowd force. Pull-in will take place otherwise. The critical AR has been calculated for each shaft diameter and is given in Table 3. Where the imposed AR was lower than the AR_{crit} in the tests, tension (pull-in) was observed in the pile. Otherwise compression was observed.

Figure 12 shows that the pitch-matched installed piles show an increase in uplift capacity and stiffness with the shaft diameter. Such an increase is associated with an increase in stress magnitude around the helix (Cerfontaine *et al.*, 2020b), which can be linked to the particle displacement during installation, as shown in Figure 11c. All overflighted piles (AR = 0.5) have an identical initial greater stiffness. Their capacity is also larger than the pitch-matched installed piles, but the maximum capacity is obtained for $D_s = D_h/2$. This suggests again that the installation effect on the surrounding soil (stress and/or density) is dependent on AR. Larger D_s/D_h ratios appear to be a more optimum geometry for the single helix piles adopted here, although a better understanding of the failure mechanisms would require further experimental and numerical investigations.

3.3. Effects of pile base shape

It is assumed that a closed-ended flat base pile should have a greater penetration resistance than an asymmetric shape (cut at 45 °, see Figure 1), similar to typical onshore screw pile design (Harnish and El Naggar, 2015). Figure 13a shows that an asymmetric shape can reduce the compressive installation force by 50% for pitch-matched installation in dense (D) sand. For overflighted piles (AR = 0.5), the difference between the two base shapes is more marked at shallow depths ($z/D_h \leq 2$, Figure 13a). Beyond that depth ($z/D_h > 2$), the crowd force tends to

slightly decrease in all cases, the rate of decrease with depth being almost identical. It is assumed that the base shape affects the base penetration resistance (initial compression), but does not modify the helix behaviour (rate of variation of F_z), hence the parallel evolution of the vertical force with depth for $z/D_h > 2$. Therefore, AR_{crit} defined in Equation (14) is assumed independent of the base shape.

Figure 13b shows that the base shape effect on the torque is less dramatic than on the force for pitch-matched installation. If oveflighting leads to pull-in of the pile (MD, AR = 0.5 in Figure 13b), the torque is very similar irrespective of the base shape. On the other hand, in dense sand (D, AR = 0.5 in Figure 13b), the torque for the pile in compression (flat base) is greater than for the pile in tension (asymmetric base). This suggests that the importance of the base shape depends on the installation mechanism (compressive or pull-in crowd force).

These observations are consistent with the previous theoretical framework (section 3.1.2). Pitch-matched installation creates a flow around mechanism during installation and requires a large compressive force. Therefore, the base shape influences the penetration resistance. Piles which are sufficiently overflighted ($AR<AR_{crit}$) reduce the stress magnitude under the helix (Figure 4, Figure 10). The upwards movement of particles becomes the dominant mechanism. Therefore, base penetration is only important during the shallow penetration of the pile, because the helix must reach a minimum embedment before the pull-in becomes effective.

4. Installation force prediction framework

The centrifuge results have shown that screw piles can be in compression or in tension as a function of the imposed AR. The AR which marks the transition from compressive to pull-in force is smaller than one (AR_{crit}). Previous predictive models (Tsuha and Aoki, 2010; Sakr, 2015; Davidson *et al.*, 2020; Spagnoli *et al.*, 2020) were based on pitch-matched installation

and only consider a helix in compression. This section introduces a new framework to predict the potential for a helix geometry to generate some pull-in and its magnitude.

4.1. Shaft penetration resistance

The shaft penetration resistance can be estimated based on the CPT methodology proposed by Al-Baghdadi *et al.* (2017) and updated by Davidson *et al.*, (2018) and ultimately by Davidson *et al.* (2020). In this method, it is assumed that the radial stress acting on the shaft (σ_r) at a given depth is proportional to the cone penetration resistance at the same depth ($\bar{q}_c$, obtained by averaging of q_c over z $\pm D_h$)

$$\sigma_r = a\bar{q}_c \tag{15}$$

where *a* is the stress drop index ($a = 0.03$) (Lehane *et al.*, 2007). The total shaft force (F_s) component can be obtained by numerically integrating the vertical shear stress (τ_z, Equation 5) along the pile embedded length, including the dependence on AR, as discussed in section (3.1).

$$F_s = \sum \tau_z \pi D_s \, dH = \frac{1}{\sqrt{1 + p_i^2}} \pi D_s \left(a \tan \delta_{crit} \sum \bar{q}_c \; dH \right) \tag{16}$$

where p_i is the installation pitch defined in Equation 6.

4.2. Helix and base vertical forces

The model piles used in the centrifuge tests were not instrumented and the exact base and helix contributions were not directly measured. However, a framework was proposed for the helix behaviour prediction, which is consistent with the different macroscopic observations, theoretical reasoning as well as previous DEM observations (Sharif *et al.*, 2020a). It must be noted that further tests with instrumented piles or micromechanical investigations are necessary to fully validate these hypotheses.

The shaft penetration resistance calculated by Equation (16) varies between 0.015MN and 0.27MN, with a median value of 0.13MN. This means that the helix (and base) behaviour is

dominant when the pile experiences a significant pull-in or compressive force, one order of magnitude greater than the shaft penetration resistance. If the imposed AR is close to AR_{crit}, the measured vertical force is close to zero and there is an equilibrium between the helix pull-in and the base and shaft penetration resistances. The total recorded vertical force (F_z) was corrected by removing the shaft penetration resistance (Figure 14), in order to highlight the behaviour of helix and base only ($F_{z,corr}$).

When $AR<AR_{crit}$ (pile in tension), the pile base and helix create two different mechanisms in the soil: the base penetrates the soil and the helix moves particles upwards. The pile behaviour can be idealised as follows (Figure 15). The corrected force is slightly in compression during the first meters. The pile base penetration resistance (F_b) increases, but the overflighting mechanism has not fully kicked in, because the helix is too close to the surface (insufficient helix capacity to oppose the upwards movement of particles). When z/D_h >3, the corrected force in tension increases almost linearly with depth, as the helix pull-in (F_h) dominates the pile behaviour. It is believed that the overflighting effect, by moving particles upwards, reduces the pile base penetration resistance, which becomes almost constant. Consequently, the variation of the corrected force with depth ($\Delta F_{z,corr}$) is equal to the variation of the helix force (ΔF_h).

When $AR>AR_{crit}$ (pile in compression), the corrected force is slightly non-linear over the first penetration meters (Figure 15), then increases almost linearly with depth. It is not possible to distinguish between base and helix components in this case, as they both contribute to the same flow around mechanism.

4.3. Helix factor

The rate of variation of the corrected vertical force with depth ($\Delta F_{z,corr}/\text{unit depth}$) can be calculated for the different tests by a linear regression over a range of depths where the evolution is quasi-linear ($z/D_h>3$, e.g. in Figure 15). Those results can be normalised as a helix factor (N_h)

$$N_h = \frac{\Delta F_{z,corr}/\text{unit depth}}{A_{eff}} \quad (17)$$

where A_{eff} is an efficient area related to the active mechanism, equal to $\pi D_h^2/4$ when the pile creates a flow around mechanism (rate of variation generates compression) and $\pi(D_h^2 - D_c^2)/4$ when the pile creates some pull-in. The normalised pull-in factor N_h is depicted in Figure 16 as a function of a normalised advancement ratio AR^*, defined as

$$AR^* = \frac{AR}{AR_{crit}} \tag{18}$$

where AR_{crit} is the critical advancement ratio defined in Equation (14). Figure 16 shows that the helix factors on the pull-in side lie in a relatively narrow range as a function of AR^* and seem to converge asymptotically towards a maximum value, which is consistent with previous observations (see section 3.1). The helix factor decreases to zero (i.e. transition from pull-in to compressive vertical force) for a normalised ratio close to 0.8. This suggests Equation (14) overestimates the value of the critical advancement ratio (AR_{crit}). This could be due to the hypothesis of a constant soil volume displacement to define the AR_{crit} and could be corrected by investigating a soil compressibility effect. On the contrary, the helix factor is greater in magnitude and does not show any asymptotic behaviour on the compressive side in the range of installation parameters investigated. There are more variations between the different tests for a constant AR^*, because of base and shaft effects on the flow around failure mechanism.
The pull-in side of this figure has more practical interest, as the helix factor describes the helix pull-in potential. This framework enables the prediction of a refusal during installation, i.e. the depth where the shaft penetration resistance will become greater than the combined helix pull-in and reaction forces. An envelope as defined by equation (19) can be used to describe the non-dimensional helix factor (N_h) on the pull-in side,

$$N_h = N_{h,lim}\left(1 - \left(\frac{AR^*}{AR^*_{lim}}\right)^{\alpha}\right)^{\frac{1}{\alpha}} \tag{19}$$

where $N_{h,lim}$ is the asymptotic value of the helix factor, AR^*_{lim} is the normalised ratio marking the transition from pull-in to compressive crowd force and α is a shaping parameter. Such mathematical formulation is similar to a generalised envelope failure surface for foundations under combined (V-H or V-M) loading (Taiebat and Carter, 2000), whilst maintaining a relatively low number of parameters before calibration and implementation. The envelope was traced in Figure 16 on the pull-in side based on visual inspection of the datapoints and general agreement of experimental results and predictions. The fitting parameters related to each sand density are given in Table 4. Similar envelopes were traced manually on the compression side, but they have low interest as large reaction forces are impractical. These results were obtained in dry sand and remain valid in saturated sand, provided that the sand behaviour is drained (slow installation rate and/or high permeability). The undrained overflighting movement of the helix would probably increase the pore water pressure in the sand rather than increase sand density or effective stress field. Therefore, an undrained installation could limit the tensile capacity enhancement. However, additional tests are necessary to understand this installation rate effect.

5. Potential for pile/anchor improved design

Experimental findings and analytical modelling described in this paper suggest that there could be a great potential for screw pile improved design, especially for offshore applications where tensile capacity/stiffness is critical. However, additional small-scale model and field tests are necessary to further validate the results and change design practice.

- Overflighting below recommendations (advancement ratio, AR<0.8) during installation in sand could be encouraged for anchoring applications, where the uplift capacity and stiffness are critical, provided the sand behaves in a drained manner.
- The AR alone is insufficient to predict the development of pull-in during the installation. The shaft to helix diameter ratio (D_s/D_h) and tip shape should be also be considered.

- An optimum shaft diameter (at a given AR) can be found to minimise the installation requirements whilst maximising the uplift capacity. However, additional tests are necessary to evaluate the relationship between the AR, the D_s/D_h ratio, the embedment depth and soil relative density.
- Some compressive crowd force is necessary at the beginning of the installation to engage the helix into the ground and should be reduced by minimising the base penetration resistance (axisymmetric and/or open-ended geometry).
- The torque correlation factor (k_T^*) was shown to be dependent on the relative density and AR, and cannot be considered as a constant value for a given geometry.
- Any restriction of the pile vertical movement (e.g. lifting by a crane) should be done carefully, as the pull-in force generated could destabilise the installation equipment.
- A reduced AR can increase the uplift capacity, but also reduce the compressive capacity, as shown by Sharif *et al.* (2020a). Therefore, caution must be exercised if the pile is subjected to both tension and compression loading.

6. Conclusion

This paper investigates the effect of installation parameters on the installation requirements (force and torque) as well as the uplift capacity of screw piles. Nineteen centrifuge tests have been undertaken, varying the screw pile geometry (shaft diameter and base shape), advancement ratio (AR) and sand bed relative density.

It was previously shown by other researchers that the compressive (crowd) force necessary to install screw piles for offshore applications would be near impossible to achieve in the field, if the advancement ratio was maintained above 0.8, as recommended by all standards. However, it was shown in this paper that overflighted installation below the recommended AR significantly reduced the necessary crowd force and increased the (shallow) uplift

capacity/stiffness of the piles in sand, while the torque was not significantly increased. These observations together with the 'silent' installation of screw piles make them a promising technology for foundations/anchoring of floating offshore devices. *Although the potential beneficial effects of reducing AR on single helix screw pile performance have been demonstrated herein through centrifuge physical modelling, further confidence for full scale deployment would be gained through field scale demonstration of these observations. Finally, t*he extrapolation of those results to clayey soils should be avoided, as the methodology has not been tested in this case.

A theoretical qualitative model was developed to explain the effect of AR on the pile installation force and torque. Overflighting a pile (AR < 1) actively displaces soil particles above the helix upwards during installation. The surrounding soil acts as a non-linear spring progressively compressed by the particles moving upwards, which creates a pull-in force acting on the helix. Overflighting at AR < 1 is a necessary but not sufficient condition to create a pull-in effect. The centrifuge results highlighted that increasing the shaft to helix diameter ratio impeded the pull-in effect. A critical advancement ratio, depending on the shaft to helix diameter ratio, was defined to mark the transition between pull-in and compressive behaviour of the pile.

An empirical helix factor was introduced to describe the pull-in potential of screw piles as a function of a normalised advancement ratio (AR^*). A single helix factor was calculated for each test. Factors on the pull-in side of the pile were shown to increase asymptotically to a maximum value as AR^* is reduced and could be described by a mathematical formula, which only depends on soil density. However, additional tests using instrumented piles are necessary to refine the interpretation of results and quantify the split of penetration resistance between the shaft, the helix and the base of the pile.

7. Acknowledgements

This project received funding from the European Union's Horizon 2020 research and innovation programme under the Marie Sklodowska-Curie grant agreement No 753156. The authors would like to acknowledge the support of the Engineering and Physical Science Research Council (EPSRC) (Grant no. EP/N006054/1: Supergen Wind Hub Grand Challenges Project: Screw piles for wind energy foundations) and the EPSRC NPIF funded studentship with industrial support from Roger Bullivant Limited.

8. Notation

a	Stress drop index, from (Lehane *et al.*, 2007)
AR	Advancement ratio
AR_{crit}	Critical advancement ratio
AR^*	Normalised advancement ratio
AR^*_{lim}	Normalised advancement ratio at transition between compressive and tensile pile behaviours
D_h	Helix diameter
D_r	Relative density
D_s	Shaft diameter
F_b	Resultant force acting on the base
F_{const}	Crowd force applied during the constant force installation
F_h	Resultant force acting on the helix
F_s	Resultant force acting on the shaft
F_z	Total vertical force
$F_{z,corr}$	Vertical force measured during centrifuge tests without shaft contribution

$F_{z,u}$	Uplift capacity
H	Embedment depth of the helix
k_T^*	Non-dimensional torque correlation factor
N_γ	Helix non-dimensional breakout factor
N_h	Non-dimensional helix factor
$N_{h,lim}$	Asymptotic value of the non-dimensional helix factor N_h
p_h	Helix pitch
p_i	Installation pitch
$\bar{q}_c$	Averaged cone penetration resistance
T_b	Torque acting on the base
t_h	Helix plate thickness
T_h	Torque acting on the helix
T_s	Resultant force acting on the torque
T_z	Total torque
v_h	Horizontal instantaneous velocity of the pile during installation
v_i	Instantaneous velocity of the pile during installation
v_z	Vertical instantaneous velocity of the pile during installation
z	Depth
γ'	Buoyant unit weight (=dry weight in this study)
δ_{crit}	Critical state interface friction angle
$\Delta F_{z,corr}$	Variation of the corrected vertical force $F_{z,corr}$
Δz_h	Vertical displacement of the helix after one helix revolution
Δz_p	Vertical displacement of the particle in contact with the helix after one helix revolution
σ_r	Radial stress acting along the shaft
τ_h	Horizontal component of the shear stress

τ_{max}	Maximum shear stress
τ_z	Vertical shear stress
ω	Pile rotation rate during installation

9. References

Al-Baghdadi, T. (2018) *Screw piles as offshore foundations: Numerical and physical modelling. PhD thesis.* University of Dundee, UK.

Al-Baghdadi, T. A., Brown, M. J. and Knappett, J. A. (2016) Development of an inflight centrifuge screw pile installation and loading system, in *Proceedings of the 3rd European Conference on Physical Modelling in Geotechnics (EUROFUGE 2016)*. Nantes, France, 1-3June 2016.

Al-Baghdadi, T. A. T., Davidson, C., Brown, M. J. M., Knappett, J. J. A., Brennan, A., Augarde, C., Coombs, W., Wang, L., Richards, D. and Blake, A. (2017) CPT based design procedure for installation torque prediction for screw piles installed in sand, *8th International Conference on Offshore Site Investigation & Geotechnics*. London, UK: Society for Underwater Technology, (1), pp. 346–353. doi: 10.3723/osig17.346.

Al-Defae, A. H., Caucis, K. and Knappett, J. A. A. (2013) Aftershocks and the whole-life seismic performance of granular slopes, *Géotechnique*, 63(14), pp. 1230–1244. doi: 10.1680/geot.12.P.149.

Al-Defae, A. H. H. (2013) *Seismic Performance of Pile-Reinforced Slopes. PhD thesis.* University of Dundee.

Bailey, H., Senior, B., Simmons, D., Rusin, J., Picken, G. and Thompson, P. M. (2010) Assessing underwater noise levels during pile-driving at an offshore windfarm and its potential effects on marine mammals, *Marine Pollution Bulletin*, 60(6), pp. 888–897. doi: 10.1016/j.marpolbul.2010.01.003.

Bolton, M. D. (1986) The strength and dilatancy of sands, *Géotechnique*, 36(1), pp. 65–78.

doi: 10.1680/geot.1986.36.1.65.

Bolton, M. D., Gui, M. W., Garnier, J., Corte, J. F., Bagge, G., Laue, J. and Renzi, R. (1999) Centrifuge cone penetration tests in sand, *Géotechnique*, 49(4), pp. 543–552. doi: 10.1680/geot.1999.49.4.543.

Bradshaw, A. S., Zuelke, R., Hildebrandt, L., Robertson, T. and Mandujano, R. (2018) Physical modelling of a helical pile installed in sand under constant crowd, in Davidson, C., Knappett, J. A., Brown, M. J., Brennan, A. J., Augarde, C., Coombs, W., Wang, L., Richards, D., White, D., and Blake, A. (eds) *Proceedings of the 1st International Symposium on Screw Piles for Energy Applications (ISSPEA)*. Dundee, UK, pp. 109–115. doi: https://doi.org/10.20933/100001123.

BS8004:2015 (2015) Code of practice for foundations. BSI Standards Limited.

Byrne, B. W. and Houlsby, G. T. (2015) Helical piles: An innovative foundation design option for offshore wind turbines, *Philosophical Transactions of the Royal Society A: Mathematical, Physical and Engineering Sciences*, 373(2035), pp. 1–11. doi: 10.1098/rsta.2014.0081.

Cerfontaine, B., Knappett, J. A., Brown, M. J. and Bradshaw, A. S. (2019) Effect of soil deformability on the failure mechanism of shallow plate or screw anchors in sand, *Computers and Geotechnics*, 109(May), pp. 34–45. doi: https://doi.org/10.1016/j.compgeo.2019.01.007.

Cerfontaine, B., Knappett, J. A., Brown, M. J., Davidson, C. and Sharif, Y. (2020a) Optimised design of screw anchors in tension in sand for renewable energy applications, *(accepted for publication in) Ocean Engineering*, 217(c).

Cerfontaine, B., Knappett, J., Brown, M. J., Davidson, C., Al-Baghdadi, T., Brennan, A., Augarde, C., Coombs, W., Wang, L., Blake, A., Richards, D. and Ball, J. (2020b) A Finite Element approach for determining the full load-displacement relationship of axially-loaded screw anchors, incorporating installation effects, *Canadian Geotechnical Journal*. doi: https://doi.org/10.1139/cgj-2019-0548.

Cerfontaine, B., Sharif, Y. U. and Davidson, C. (2021) Centrifuge dataset for screw pile

installation and uplift. Dundee: University of Dundee. doi: https://doi.org/10.15132/10000160.

Davidson, C., Al-Baghdadi, T., Brown, M., Brennan, A., Knappett, J., Augarde, C., W., C., Wang, L., Richards, D., Blake, A. and Ball, J. (2018) A modified CPT based installation torque prediction for large screw piles in sand, in Hicks, M., Pisanò, F., and Peuchen, J. (eds) *Cone Penetration Testing*. Delft, The Netherlands. doi: https://doi.org/10.1201/9780429505980.

Davidson, C., Brown, M. J., Cerfontaine, B., Al-Baghdadi, T., Knappett, J., Brennan, A., Augarde, C., Coombs, W., Wang, L., Blake, A., Richards, D. and Ball, J. (2020) Physical modelling to demonstrate the feasibility of screw piles for offshore jacket supported wind energy structures, *Géotechnique (Published online)*. doi: 10.1680/jgeot.18.P.311.

Deeks, A. D. (2008) *An investigation into the strength and stiffness of jacked piles in sand.* University of Cambridge, UK. Available at: http://publications.eng.cam.ac.uk/328467/.

Deeks, A. D., White, D. J. and Ishihara, Y. (2010) Novel piling:Axial and rotary jacking, in *11th International Conference of the Deep Foundations Institute*. London, UK.

Ding, H., Wang, L., Zhang, P., Liang, Y., Tian, Y. and Qi, X. (2019) The recycling torque of a single-plate helical pile for offshore wind turbines in dense sand, *Applied Sciences*, 9(19), p. 4105. doi: 10.3390/app9194105.

Garnier, J., Gaudin, C., Springman, S. M., Culligan, P. J., Goodings, D., Konig, D., Kutter, B., Phillips, R., Randolph, M. F., Thorel, A., Garnier, J., Gaudin, C., Springman, S. M., Culligan, P. J., Goodings, D. *et al.* (2007) Catalogue of scaling laws and similitude questions in geotechnical centrifuge modelling, *International Journal of Physical Modelling in Geotechnics*, 7(3), pp. 01–23. doi: 10.1680/ijpmg.2007.070301.

Gavin, K., Doherty, P. and Tolooiyan, A. (2014) Field investigation of the axial resistance of helical piles in dense sand, *Canadian Geotechnical Journal*, 51(11), pp. 1343–1354. doi: 10.1139/cgj-2012-0463.

Giampa, J. R., Bradshaw, A. S. and Schneider, J. A. (2017) Influence of Dilation Angle on Drained Shallow Circular Anchor Uplift Capacity, *International Journal of Geomechanics*,

17(2), p. 4016056. doi: 10.1061/(ASCE)GM.1943-5622.0000725.

Hao, D., Wang, D., O'Loughlin, C. D., Gaudin, C., O'Loughlin, C. D. C. D. and Gaudin, C. (2019) Tensile monotonic capacity of helical anchors in sand: interaction between helices, *Canadian Geotechnical Journal*, 56(January 2019), pp. 1534–1543. doi: 10.1139/cgj-2018-0202.

Harnish, J. and El Naggar, H. M. (2015) Large Diameter Helical Pile Capacity - Torque Correlations, *Canadian Geotechnical Journal*, 54(7), pp. 968–986. doi: https://doi.org/10.1139/cgj-2016-0156.

Klinkvort, R. F., Hededal, O. and Springman, S. M. (2013) Scaling issues in centrifuge modelling of monopiles, *International Journal of Physical Modelling in Geotechnics*, 13(2), pp. 38–49. doi: http://dx.doi.org/10.1680/ijpmg.12.00010.

Komatsu, A. (2007) Development on battered pile with screw pile method (NS-ECO pile), in Kikuchi, Y., Otani, J., Kimura, M., and Morikawa, Y. (eds) *Proceedings of the International Workshop on recent advances of deep foundations (IWDPF07)*. Yokosuka, Japan.

Lauder, K. (2010) *The performance of pipeline ploughs*. University of Dundee, UK.

Lehane, B. M., Schneider, J. A. and Xu, X. (2007) Development of the UWA-05 design method for open and closed ended driven piles in siliceous sand, *Geotechnical Special Publication*, 40902(158), pp. 1–10. doi: 10.1061/40902(221)12.

Lutenegger, A. J. (2011) Historical Development of Iron Screw-Pile Foundations: 1836–1900, *The International Journal for the History of Engineering & Technology*, 81(1), pp. 108–128. doi: 10.1179/175812109x12547332391989.

Mandolini, A., Russo, G. and Viggiani, C. (2005) *Pile foundations : experimental investigations, analysis and design*, *Proceedings of the 16th International Conference on Soil Mechanics and Geotechnical Engineering*. Osaka, Japan. doi: 10.3233/978-1-61499-656-9-177.

Nagai, H., Tsuchiya, T. and Shimada, M. (2018) Influence of installation method on performance of screwed pile and evaluation of pulling resistance, *Soils and Foundations*.

Elsevier B.V., 58(2), pp. 355–369. doi: 10.1016/j.sandf.2018.02.006.

Pérez, Z. A. Z., Schiavon, J. A., Tsuha, C. H. C., Dias, D. and Thorel, L. (2018) Numerical and experimental study on influence of installation effects on behaviour of helical anchors in very dense sand, *Canadian Geotechnical Journal*, 55(8), pp. 1067–1080. doi: 10.1139/cgj-2017-0137.

Perko, H. A. (2009) *Helical Piles. A practical guide to design and installation*. 1st Edit. John Wiley & Sons, Inc. doi: 10.1002/9780470549063.

Rafsanjani, A. A. H., Salehzadeh, H. and Nuri, H. (2021) Evaluating scale effects and bearing portions in centrifuge modeling of helical anchors: Sand, *Acta Geotechnica*. Springer Berlin Heidelberg, In press. doi: 10.1007/s11440-021-01156-2.

Richards, D. J., Blake, A. P., White, D. J., Bittar, E. M. and Lehane, B. M. (2018) Field tests assessing the installation performance of screw pile geometries optimised for offshore wind applications, in Davidson, C., Knappett, J. A., Brown, M. J., Brennan, A. J., Augarde, C., Coombs, W., Wang, L., Richards, D., White, D., and Blake, A. (eds) *Proceedings of the 1st International Symposium on Screw Piles for Energy Applications (ISSPEA)*. Dunde, UK, pp. 47–54. doi: https://doi.org/10.20933/100001123.

Robinson, S., Brown, M. J., Matsui, H., Brennan, A., Augarde, C., Coombs, W. and Cortis, M. (2019) Centrifuge testing to verify scaling of offshore pipeline ploughs, *International Journal of Physical Modelling in Geotechnics*, 19(6), pp. 305–317. doi: 10.1680/jphmg.17.00075.

Sakr, M. (2015) Relationship between installation torque and axial capacities of helical piles in cohesionless soils, *Canadian Geotechnical Journal*, 52(6), pp. 747–759. doi: 10.1139/cgj-2013-0395.

Schiavon, J. A. (2016) *Comportamento de ancoragens helicoidais submetidas a carregamentos cíclicos. PhD Thesis*. University of São Paulo, Brazil.

Schiavon, J. A., Tsuha, C. H. C., Neel, A. and Thorel, L. (2016a) Physical modelling of a single-helix anchor in sand under cyclic loading, *EUROFUGE 2016 3rd European conference on*

Physical Modelling in Geotechnics, (June), pp. 275–279.

Schiavon, J. A., Tsuha, C. H. C. and Thorel, L. (2016b) Scale effect in centrifuge tests of helical anchors in sand, *International Journal of Physical Modelling in Geotechnics*, 16(4), pp. 185–196. doi: 10.1680/jphmg.15.00047.

Sharif, Y. U., Brown, M. J., Cerfontaine, B., Davidson, C., Ciantia, M., Knappett, J., Brennan, A., Ball, J. D., Augarde, C., Coombs, W., Blake, A., Richards, D., White, D., Huisman, M. and Ottolini, M. (2020a) Effects of screw pile installation on installation requirements and in-service performance using the Discrete Element Method, *Canadian Geotechnical Journal (published online)*. doi: 10.1139/cgj-2020-0241.

Sharif, Y. U., Brown, M. J., Ciantia, M. O., Cerfontaine, B., Davidson, C., Knappett, J., Meijer, G. J. and Ball, J. (2020b) Using DEM to create a CPT based method to estimate the installation requirements of rotaty installed piles in sand, *Canadian Geotechnical Journal (published online)*. doi: 10.1139/cgj-2020-0017.

Shi, D., Yang, Y., Deng, Y. and Xue, J. (2019) DEM modelling of screw pile penetration in loose granular assemblies considering the effect of drilling velocity ratio, *Granular Matter*. Springer Berlin Heidelberg, 21(3), p. 74. doi: 10.1007/s10035-019-0933-3.

Spagnoli, G., Hollanda, C. De and Tsuha, C. (2020) A review on the behavior of helical piles as a potential offshore foundation system, *Marine Georesources & Geotechnology*. Taylor & Francis, 0(0), pp. 1–24. doi: 10.1080/1064119X.2020.1729905.

Taiebat, H. A. and Carter, J. P. (2000) Numerical studies of the bearing capacity of shallow foundations on cohesive soil subjected to combined loading, *Geotechnique*, 50(4), pp. 409–418. doi: 10.1680/geot.2000.50.4.409.

Tang, C. and Phoon, K.-K. (2020) Statistical evaluation of model factors in reliability calibration of high displacement helical piles under axial loading, *Canadian Geotechnical Journal*, 57(2), pp. 246–262. doi: https://doi.org/10.1139/cgj-2018-0754.

Tsuha, C. H. C. and Aoki, N. (2010) Relationship between installation torque and uplift capacity

of deep helical piles in sand, *Canadian Geotechnical Journal*, 47(1), pp. 635–647. doi: 10.1139/T09-128.

Viggiani, C. (1989) Influenza dei fattori tecnologici sul comportamento dei pali, in *XVII Convegno nazionale dei geotecnica*. Taormina, Italy.

Wang, L., Zhang, P., Ding, H., Tian, Y. and Qi, X. (2020) The uplift capacity of single-plate helical pile in shallow dense sand including the influence of installation, *Marine Structures*. Elsevier Ltd, 71. doi: 10.1016/j.marstruc.2019.102697.

White, D. J. and Deeks, A. D. (2007) Recent research into the behaviour of jacked foundation piles, *International Workshop on Recent Advances of Deep Foundations (IWDPF07)*, (February), pp. 3–26. doi: 10.3101/1098-7096(2007)68.

Wind Europe. 2018. Offshore wind in Europe. *In* Offshore Wind in Europe: key trends and statistics 2017. doi:10.1016/S1471-0846(02)80021-X.

11. Caption list: figures

Figure 1 (a) Model pile description shown with prototype dimensions, model scale dimensions shown in brackets and (b) Plan view of strong box with pile test locations.
Figure 2 Measured vertical (crowd) force during the installation of the reference (P1) flat base screw pile in (a) dense and (b) medium-dense sand as a function of the advancement ratio (AR)
Figure 3 Split of the penetration resistance (force and torque) between the base (F_b, T_b), helix (F_h, T_h) and shaft (F_s, T_s) components and zoom on shear stress state and instantaneous velocities acting on the shaft
Figure 4 2D idealisation of the overflighting effect on particle movement. (a) Rotating and translating helix at a given depth, initial situation; (b) Rotating and translating helix after a small rotation at (AR =0.5); (c) Effect of the surrounding soil (helix embedment) on the particle movement during a small rotation (AR = 0.5). The 2D helix represents the outer edge of the helix, whose length is equal to (πD_h).
Figure 5 Relationship between the advancement ratio (Equation (6)) and (a) the installation pitch; or (b) the shear components as per Equations (4-5)
Figure 6 Measured torque during the installation of the reference (P1) flat base screw pile in (a) dense and (b) medium-dense sand as a function of the advancement ratio (AR)
Figure 7 Load-displacement during the uplift of the reference (P1) flat base screw pile in dense and medium-dense sand as a function of the advancement ratio (AR)
Figure 8 (a) Comparison of the normalised bearing factor and (b) evolution of the non-dimensional torque correlation factor, as a function of the advancement ratio (AR)
Figure 9 Idealisation of the influence of the AR during the installation (a-b) on the uplift capacity and stiffness of screw piles (c)
Figure 10 Measured (a) vertical installation force and torque (b) during the installation of screw piles P4 ($D_s = D_h/3$), P2 ($D_s = D_h/2$) and P5 ($D_s = 2D_h/3$) with the asymmetric base in dense sand as a function of the advancement ratio (AR = 0.5 or 1.0). The helix diameter ($D_h = 1.06m$) was identical in all cases.
Figure 11 Idealisation of the different installation mechanisms as a function of the volume of soil displaced by the helix (V_h) and the volume of soil displaced by the pile base penetration (V_p) during one pile rotation and helix vertical displacement (Δz_h). (a-b) Different mechanism for two piles at same AR, but different shaft diameter. (a-c) Different mechanism for same shaft diameter, but different AR. (d) Interpretation of particle displacement (AR<1).
Figure 12 Load-displacement of screw piles P4 ($D_s = D_h/3$), P2 ($D_s = D_h/2$) and P5 ($D_s = 2D_h/3$) with asymmetric base in dense sand as a function of the advancement ratio (AR = 0.5 or 1.0). The helix diameter ($D_h = 1.06m$) was identical in all cases.
Figure 13 Measured (a) vertical (crowd) force and torque (b) during the installation of screw piles P1 (flat base), P2 (asymmetric base) in medium-dense (MD) and dense (D) sand as a function of the advancement ratio (AR = 0.5 or 1.0).
Figure 14 Vertical installation force for (a) AR leading to pull-in of the pile or (b) AR leading to compression of the pile, for medium-dense (MD) and dense sand (D). Vertical forces ($F_{z,corr}$) are corrected by removing the estimated shaft penetration resistance. The test identifier is shown in brackets.
Figure 15 Idealisation of the pile vertical force-depth evolution, as a function of the shaft (F_s), base (F_b), and helix components (F_h)
Figure 16 Comparison of calculated normalised helix factors (N_h) and envelope curves (Equation 18, for tests AR<AR_{crit}), for different base shapes (flat or asymmetric), for pile P1 (flat base), P2 (asymmetric base), P4 (D_s/D_h = 1/3), P5 (D_s/D_h = 2/3), and P3 (p_h/Dh =0.52) in medium-dense (MD) and dense (D) sand.

12. Figures

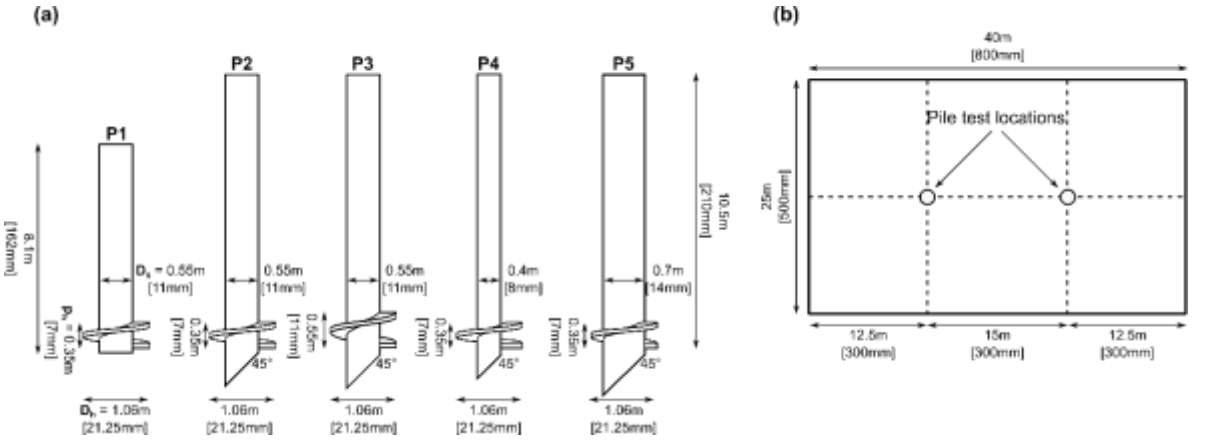

Figure 1 (a) Model pile description shown with prototype dimensions, model scale dimensions shown in brackets and (b) Plan view of strong box with pile test locations.

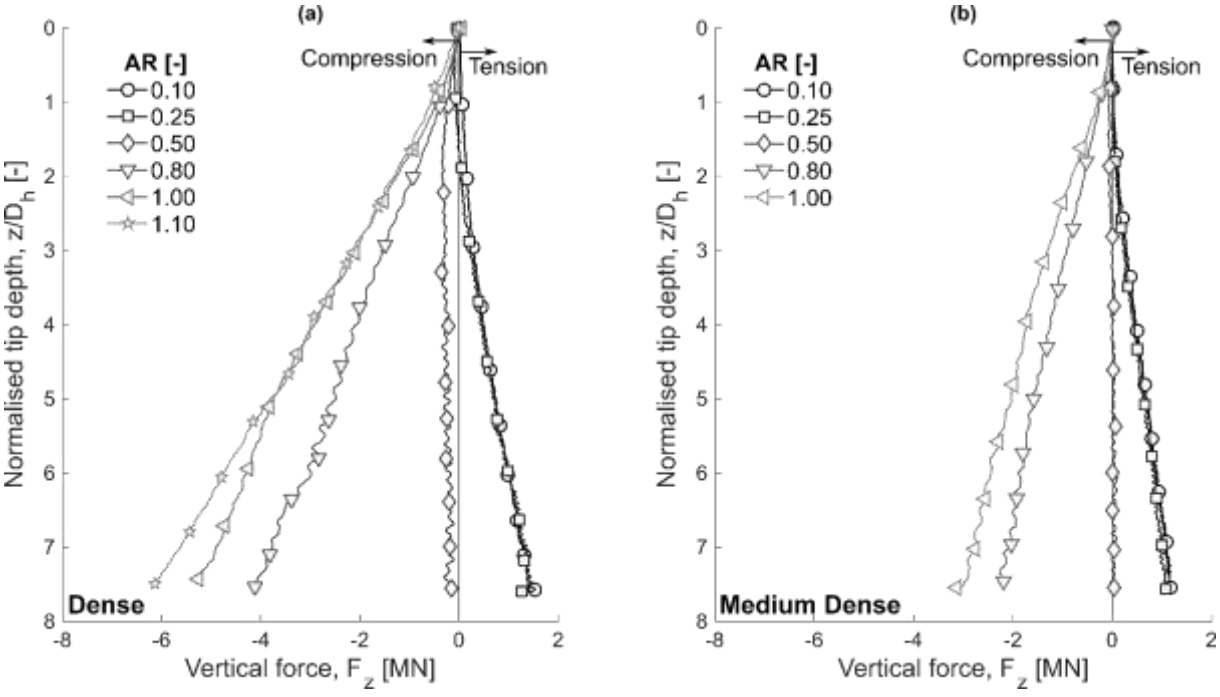

Figure 2 Measured vertical (crowd) force during the installation of the reference (P1) flat base screw pile in (a) dense and (b) medium-dense sand as a function of the advancement ratio (AR)

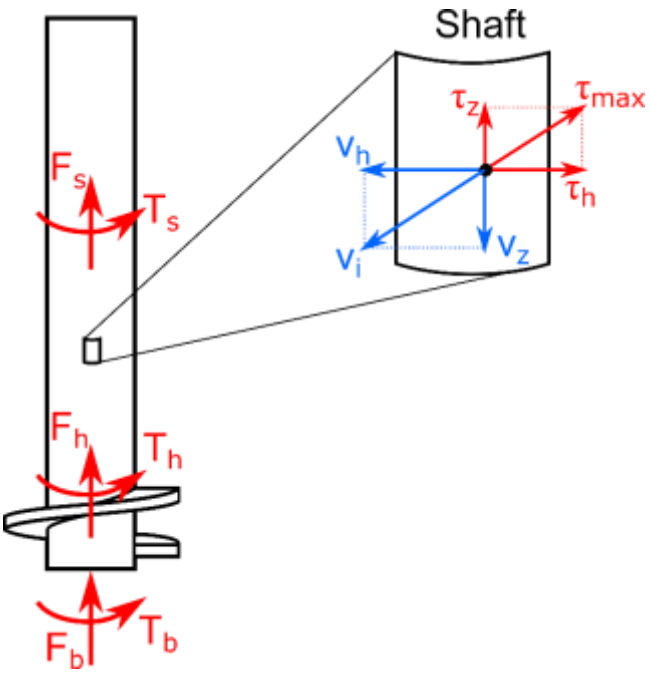

Figure 3 Split of the penetration resistance (force and torque) between the base (F_b, T_b), helix (F_h, T_h) and shaft (F_s, T_s) components and zoom on shear stress state and instantaneous velocities acting on the shaft

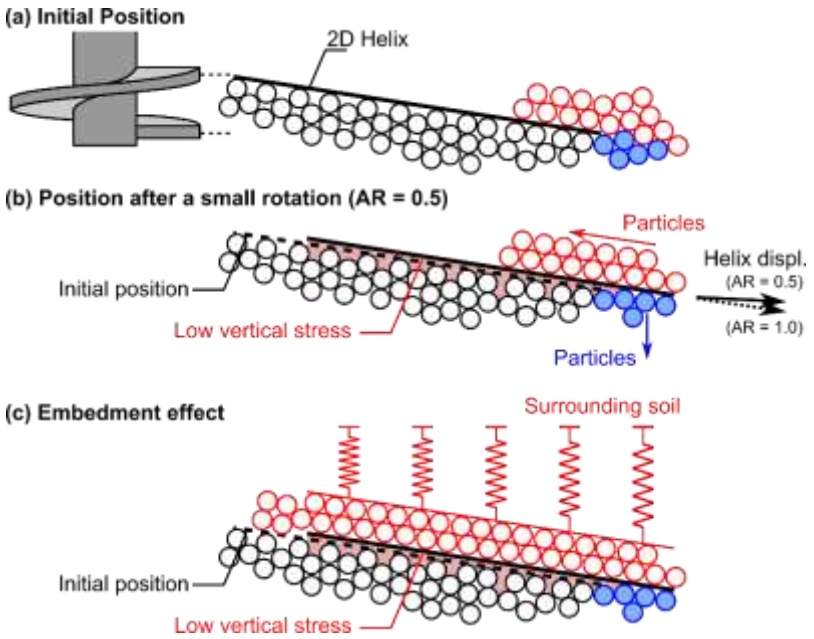

Figure 4 2D idealisation of the overflighting effect on particle movement. (a) Rotating and translating helix at a given depth, initial situation; (b) Rotating and translating helix after a small rotation at (AR =0.5); (c) Effect of the surrounding soil (helix embedment) on the particle movement during a small rotation (AR = 0.5). The 2D helix represents the outer edge of the helix, whose length is equal to (πD_h).

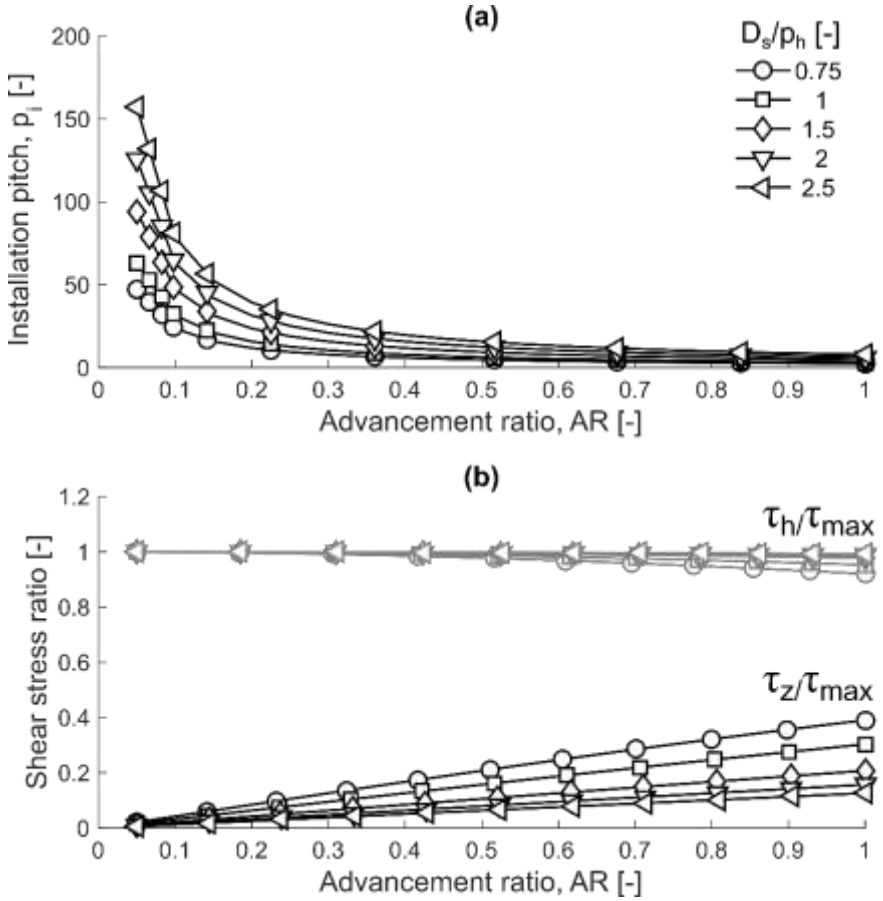

Figure 5 Relationship between the advancement ratio (Equation (6)) and (a) the installation pitch; or (b) the shear components as per Equations (4-5)

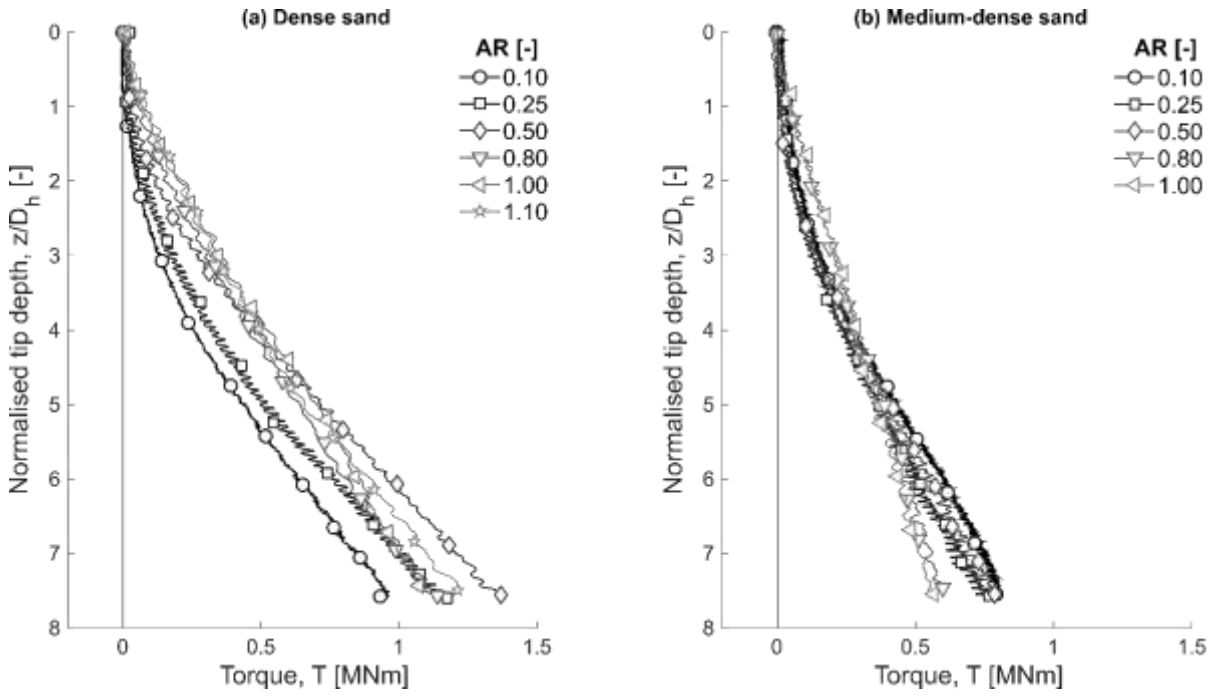

Figure 6 Measured torque during the installation of the reference (P1) flat base screw pile in (a) dense and (b) medium-dense sand as a function of the advancement ratio (AR)

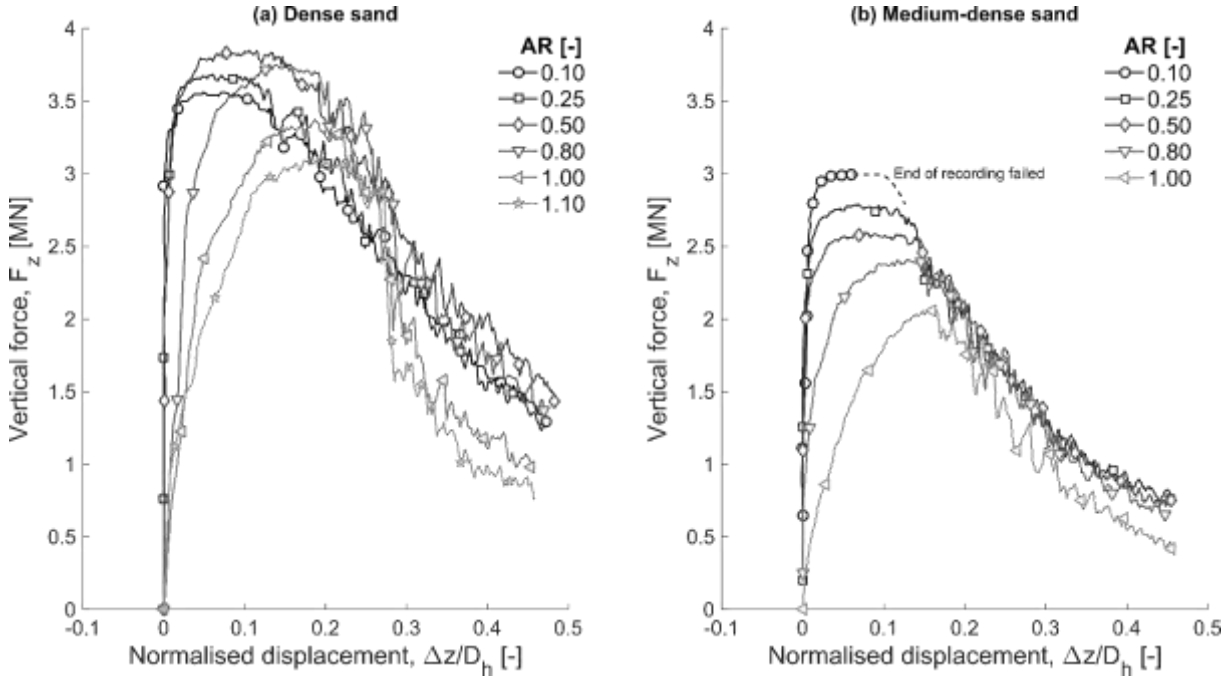

Figure 7 Load-displacement during the uplift of the reference (P1) flat base screw pile in dense and medium-dense sand as a function of the advancement ratio (AR)

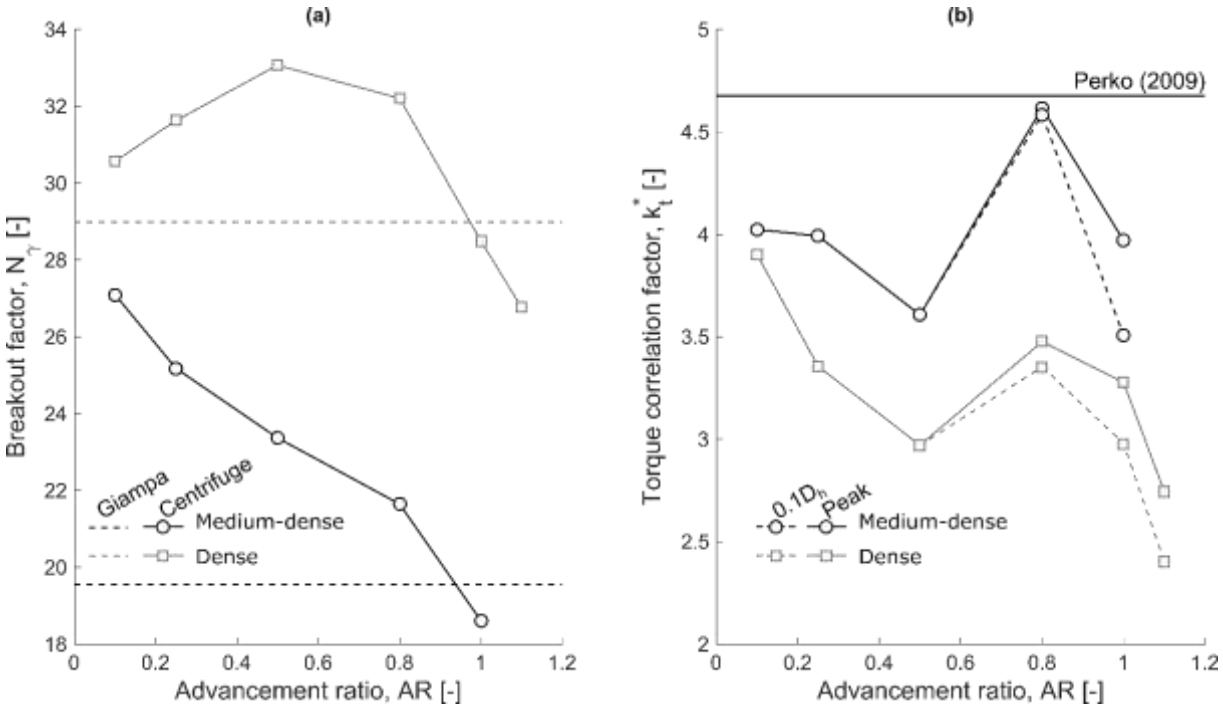

Figure 8 (a) Comparison of the normalised bearing factor and (b) evolution of the non-dimensional torque correlation factor as a function of the advancement ratio (AR), and calculated at the peak tensile force or at the force measured after 0.1Dh displacement

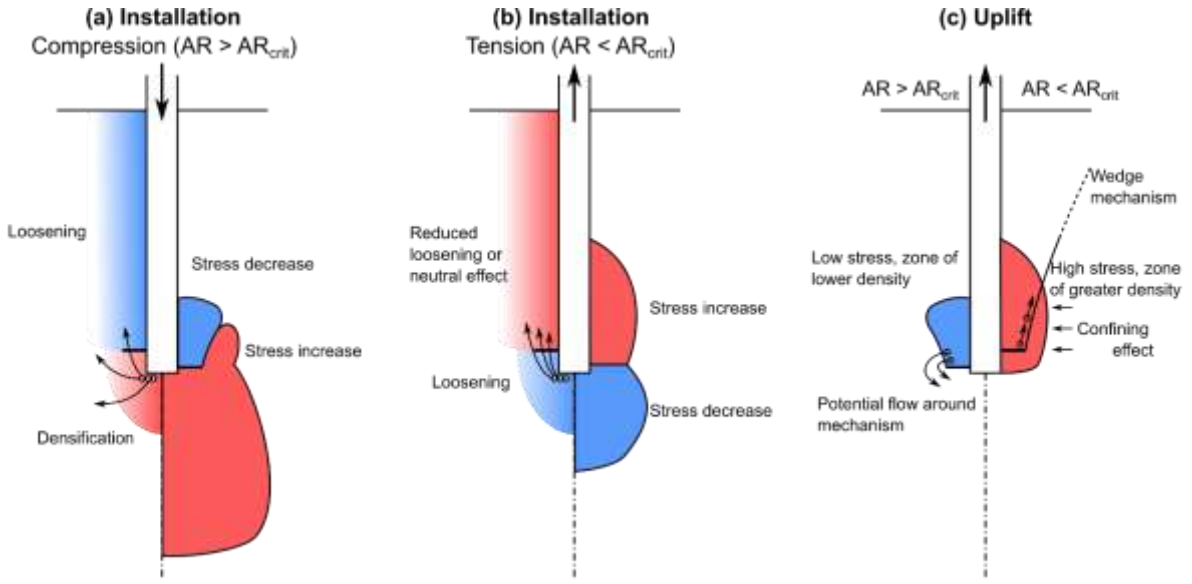

Figure 9 Idealisation of the influence of the AR during the installation (a-b) on the uplift capacity and stiffness of screw piles (c)

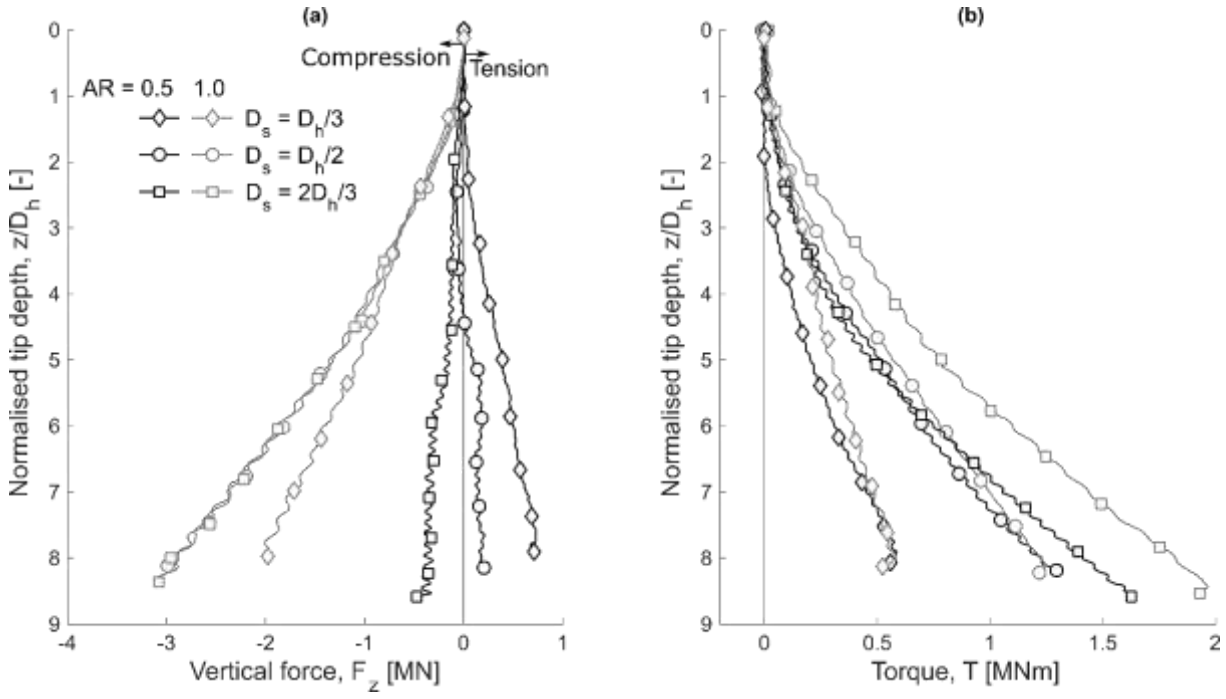

Figure 10 Measured (a) vertical installation force and torque (b) during the installation of screw piles P4 (D_s = D_h/3), P2 (D_s = D_h/2) and P5 (D_s = 2D_h/3) with the asymmetric base in dense sand as a function of the advancement ratio (AR = 0.5 or 1.0). The helix diameter (D_h = *1.06m*) was identical in all cases.

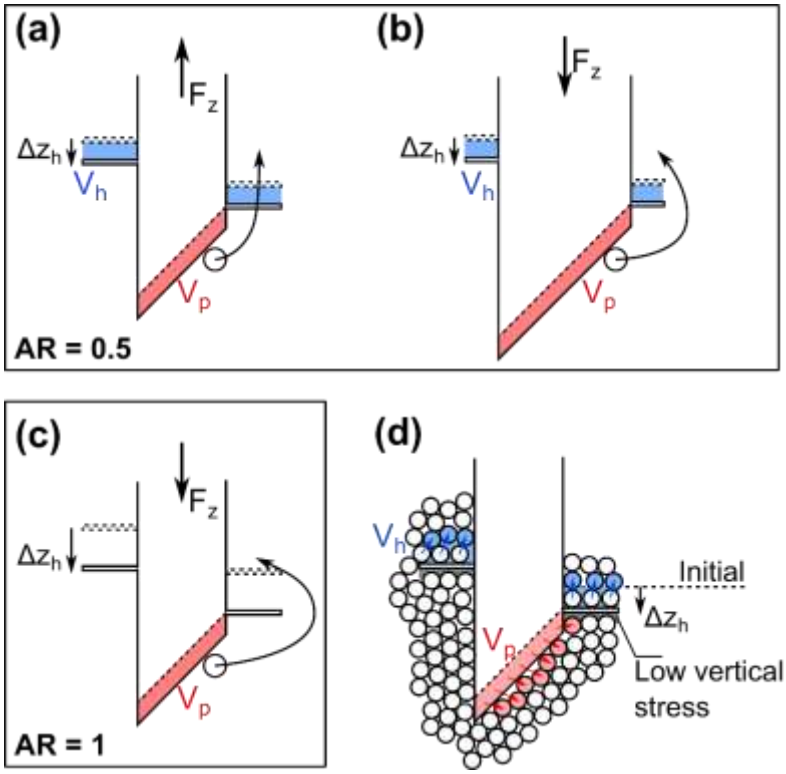

Figure 11 Idealisation of the different installation mechanisms as a function of the volume of soil displaced by the helix (V_h) and the volume of soil displaced by the pile base penetration (V_p) during one pile rotation and helix vertical displacement (Δz_h). (a-b) Different mechanism for two piles at same AR, but different shaft diameter. (a-c) Different mechanism for same shaft diameter, but different AR. (d) Interpretation of particle displacement (AR<1).

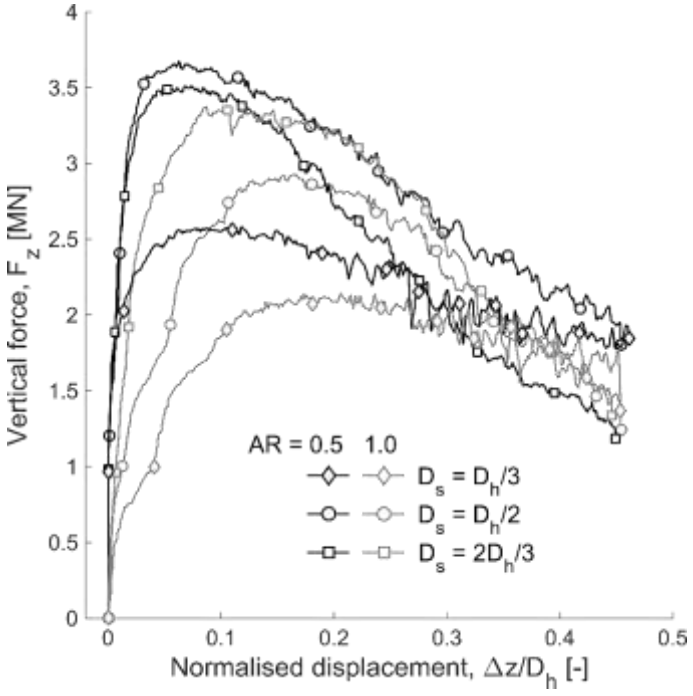

Figure 12 Load-displacement of screw piles P4 ($D_s = D_h/3$), P2 ($D_s = D_h/2$) and P5 ($D_s = 2D_h/3$) with asymmetric base in dense sand as a function of the advancement ratio (AR = 0.5 or 1.0). The helix diameter ($D_h = 1.06m$) was identical in all cases.

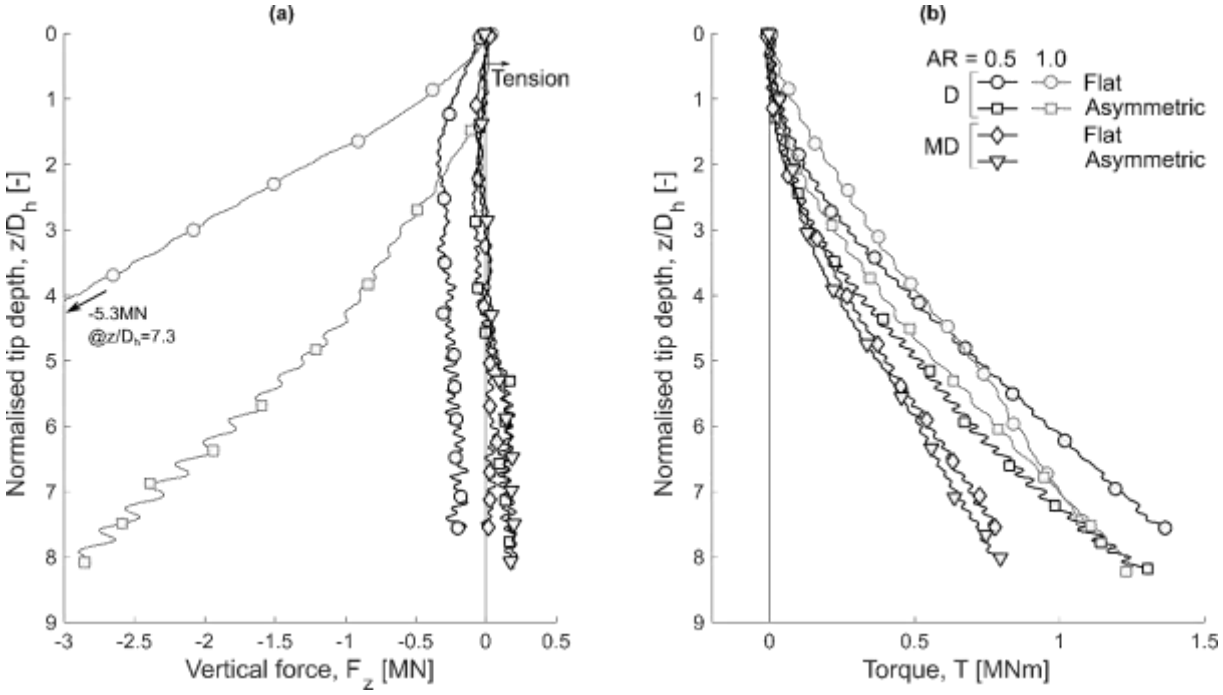

Figure 13 Measured (a) vertical (crowd) force and torque (b) during the installation of screw piles P1 (flat base), P2 (asymmetric base) in medium-dense (MD) and dense (D) sand as a function of the advancement ratio (AR = 0.5 or 1.0).

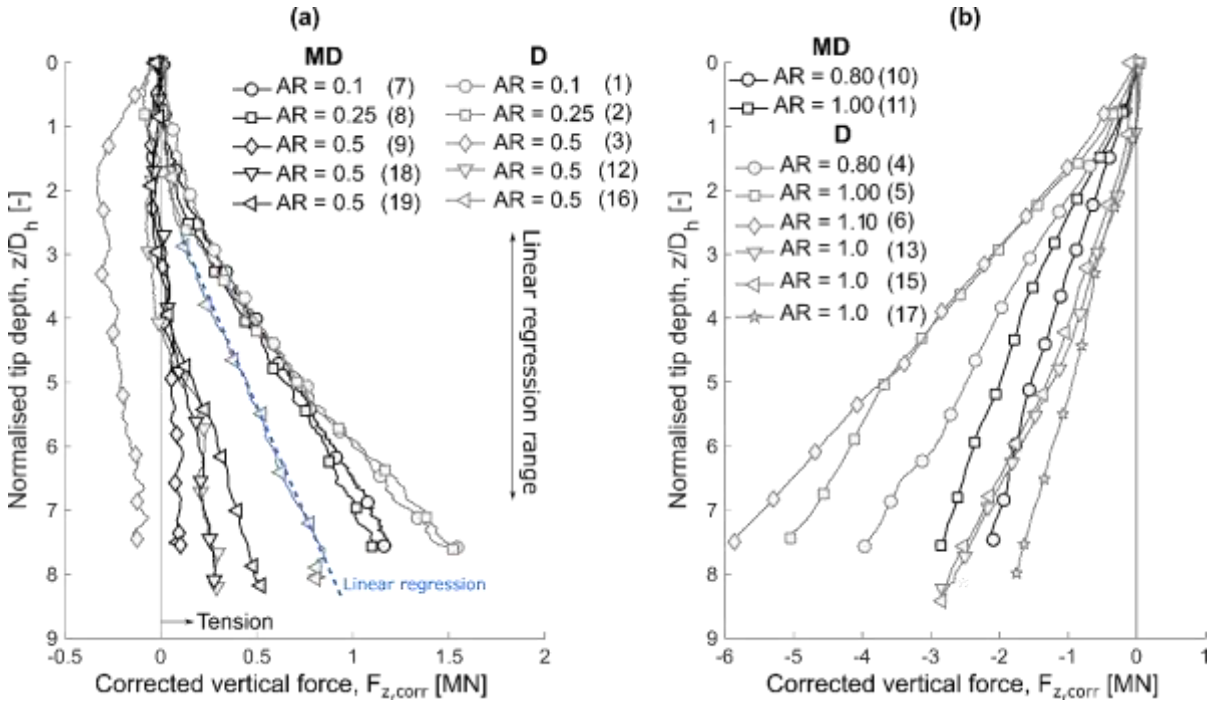

Figure 14 Vertical installation force for (a) AR leading to pull-in of the pile or (b) AR leading to compression of the pile, for medium-dense (MD) and dense sand (D). Vertical forces ($F_{z,corr}$) are corrected by removing the estimated shaft penetration resistance. The test identifier is shown in brackets.

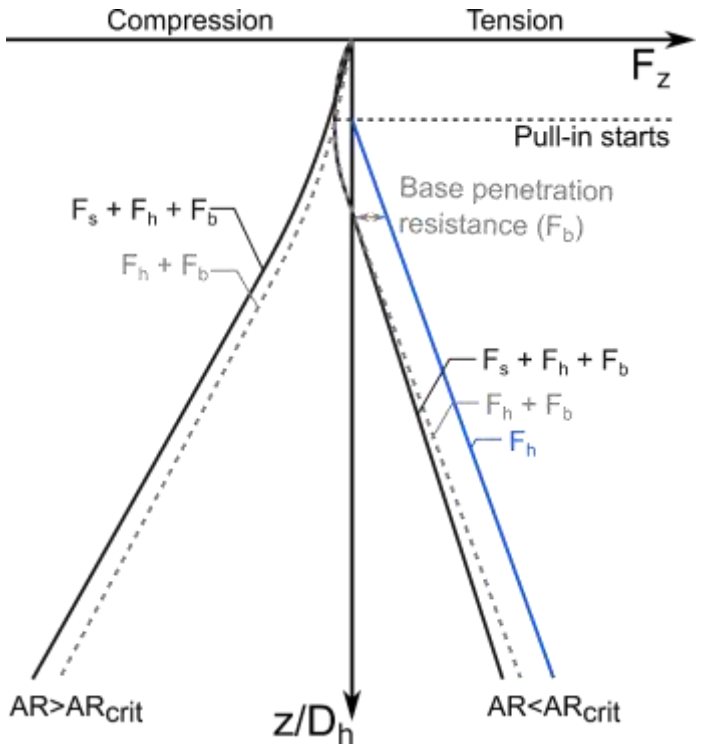

Figure 15 Idealisation of the pile vertical force-depth evolution, as a function of the shaft (F_s), base (F_b), and helix components (F_h)

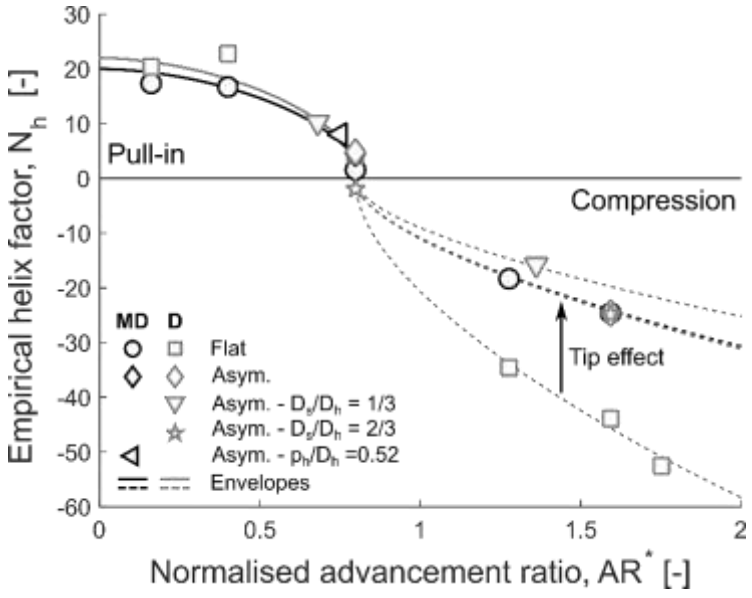

Figure 16 Comparison of calculated normalised helix factors (N_h) and envelope curves (Equation 19, for tests AR<AR$_{crit}$), for different base shapes (flat or asymmetric), for pile P1 (flat base), P2 (asymmetric base), P4 (D_s/D_h = 1/3), P5 (D_s/D_h = 2/3), and P3 (p_h/Dh =0.52) in medium-dense (MD) and dense (D) sand.

13. Caption list: tables

Table 1 Properties of the HST95 sand, after (Lauder, 2010; Al-Defae, 2013)
Table 2 List of model dimensions (prototype scale), sample relative density and installation parameters: advancement ratio (AR), helix diameter (D_h), shaft diameter (D_s), helix pitch (p_h), base shape (flat or asymmetric, i.e. cut at 45° to the horizontal direction), sand bed average relative density (D_r), final embedment depth of the base (H_{base}).
Table 3 Calculated $ARcrit$ as a function of the shaft to helix diameter ratio (D_s/D_h), measured vertical force (F_z) in the pile at the end of installation
Table 4 Parameters of the empirical model describing the helix factor on the pull-in side

14. Tables

Table 1 Properties of the HST95 sand, after (Lauder, 2010; Al-Defae, 2013)

	Symbol	**Units**	**Value**
Effective particle size	D_{10}	[mm]	0.09
Average particle size	D_{50}	[mm]	0.14
Particle specific gravity	G_s	[-]	2.63
Minimum void ratio	e_{min}	[-]	0.467
Maximum void ratio	e_{max}	[-]	0.769
Minimum dry density	ρ_{min}	[kg/m³]	1486
Maximum dry density	ρ_{max}	[kg/m³]	1793
Critical state friction angle	ϕ_{crit}	[°]	32
Sand-steel interface friction angle	δ_{crit}	[°]	24

Table 2 List of model dimensions (prototype scale), sample relative density and installation parameters: advancement ratio (AR), helix diameter (D_h), shaft diameter (D_s), helix pitch (p_h), base shape (flat or asymmetric, i.e. cut at 45° to the horizontal direction), sand bed average relative density (D_r), final embedment depth of the base (H_{base}).

ID	Pile	AR [-]	D_h [m]	D_s [m]	Ds/Dh [-]	p_h [m]	Base shape	D_r [%]	H_{base} [m]
1	P1	0.10	1.06	0.55	0.52	0.35	flat	74	7.95
2	P1	0.25	1.06	0.55	0.52	0.35	flat	73	7.95
3	P1	0.50	1.06	0.55	0.52	0.35	flat	75	7.95
4	P1	0.80	1.06	0.55	0.52	0.35	flat	73	7.95
5	P1	1.00	1.06	0.55	0.52	0.35	flat	73	7.95
6	P1	1.10	1.06	0.55	0.52	0.35	flat	73	7.95
7	P1	0.10	1.06	0.55	0.52	0.35	flat	52	8.05
8	P1	0.25	1.06	0.55	0.52	0.35	flat	53	8.05
9	P1	0.50	1.06	0.55	0.52	0.35	flat	52	8.05
10	P1	0.80	1.06	0.55	0.52	0.35	flat	53	8.05
11	P1	1.00	1.06	0.55	0.52	0.35	flat	52	8.05
12	P2	0.50	1.06	0.55	0.52	0.35	Asymmetric	78	8.65
13	P2	1.00	1.06	0.55	0.52	0.35	Asymmetric	78	8.65
14	P5	0.50	1.06	0.7	0.66	0.35	Asymmetric	73	9.05
15	P5	1.00	1.06	0.7	0.66	0.35	Asymmetric	73	9.05
16	P4	0.50	1.06	0.4	0.38	0.35	Asymmetric	73	8.45
17	P4	1.00	1.06	0.4	0.38	0.35	Asymmetric	73	8.45
18	P2	0.50	1.06	0.55	0.52	0.35	Asymmetric	52	8.65
19	P3	0.50	1.06	0.55	0.52	0.55	Asymmetric	52	8.60

Table 3 Calculated AR_{crit} as a function of the shaft to helix diameter ratio (D_s/D_h), measured vertical force (F_z) in the pile at the end of installation

D_s/D_h [-]	AR_{crit} [-]	Imposed AR [-]	Observed F_z
1/3	0.76	0.5	Tension
1/2	0.64	0.5	Tension
2/3	0.48	0.5	Compression

Table 4 Parameters of the empirical model describing the helix factor on the pull-in side

	$N_{h,lim}$ [-]	AR^*_{lim} [-]	α [-]	$AR^*_{cut-off}$ [-]
Medium-dense	20	0.82	1.75	0.6
Dense	22	0.82	1.75	0.6